Summer 8-3-2016

DEVELOPMENT OF ECO-FRIENDLY COMPOSITE FOAM BOARDS FOR THERMAL INSULATION AND PACKAGING PURPOSES USING CELLULOSE NANOFIBRILS (CNF)

Nadir Yildirim

DEVELOPMENT OF ECO-FRIENDLY COMPOSITE FOAM BOARDS FOR THERMAL INSULATION AND PACKAGING PURPOSES USING CELLULOSE NANOFIBRILS (CNF)

By

Nadir Yildirim

B.Sc. Karadeniz Technical University, 2007

M.Sc. Mugla University, 2010

A DISSERTATION

Submitted in Partial Fulfillment of the

Requirements for the Degree of

Doctor of Philosophy

(in Forest Resources)

The Graduate School

The University of Maine

August 2016

Advisory Committee:

Dr. Stephen M. Shaler, Professor of Wood Science, Advisor

Dr. Douglas Gardner, Professor of Forest Operations, Bioproducts & Bioenergy

Dr. Douglas W. Bousfield, Professor of Chemical & Biological Engineering

Dr. Roberto Lopez-Anido, Professor of Civil & Environmental Engineering

Dr. Robert Rice, Professor of Wood Science & Technology

DISSERTATION ACCEPTANCE STATEMENT

On behalf of the Graduate Committee for Nadir Yildirim, I affirm that this manuscript is the final and accepted dissertation. Signatures of all committee members are on file with the Graduate School at the University of Maine, 42 Stodder Hall, Orono, Maine.

Stephen M. Shaler, Professor of Wood Science August 3, 2016

COPYRIGHT NOTICE

LIBRARY RIGHTS STATEMENT

In presenting this dissertation in partial fulfillment of the requirements for an advanced degree at the University of Maine, I agree that the Library shall make it freely available for inspection. I further agree that permission for “fair use” copying of this dissertation for scholarly purposes may be granted by the Librarian. It is understood that any copying or publication of this dissertation for financial gain shall not be allowed without my written permission.

Signature: _____

Date: _____

DEVELOPMENT OF ECO-FRIENDLY COMPOSITE FOAM BOARDS FOR THERMAL INSULATION AND PACKAGING PURPOSES USING CELLULOSE NANOFIBRILS (CNF)

By Nadir Yildirim

Thesis Advisor: Dr. Stephen M. Shaler

An Abstract of the Dissertation Presented
in Partial Fulfillment of the Requirements for the
Degree of Doctor of Philosophy
(in Forest Resources)
August 2016

Reducing energy consumption is a high priority in the United States and throughout the world. Energy used to heat and cool occupied constructed facilities is of particular concern, and one of the most effective strategies is insulating the building envelope. Historically, builders used whatever material was available to fill the void between interior and exterior walls, including wool fibers, paper, and even corn cobs. Today, homes are built using foam insulation that harden when applied, blown-in loose insulation, fiberglass mats or rigid foam boards usually composed of polystyrene. Rigid foam boards are used in a variety of applications despite the fact that they typically contain non bio-based materials, require substantial amount of energy to produce, and are not easily recycled. A new “green” insulation material is needed that uses a new raw

material and a new process to create its structure. In this study cellulose nanofibrils (CNF) were used as the raw material and industrial corn-starch was used as a binder that uses hydrogen bonding for cross linking to create a successful thermal insulation foam board.

Cellulose, one of the most ubiquitous and abundant renewable polymers on the planet, can be obtained from a variety of sources including trees, agricultural crops, bacteria, and even from animals. The material's abundance and properties have increased research on cellulose and its derivatives in recent years.

Cellulose nanofibrils are organic polymers that can be obtained through chemical or mechanical methods. The CNF used in this study was produced by the mechanical breakdown of softwood cellulose fibers.

Starch is an abundant green polymer and is a promising raw component for the development of novel materials. However, starch has low mechanical properties. In this research, industrial corn starch was reinforced with CNF suspensions through a unique freeze-drying technique. The research showed significant improvement in the mechanical properties and micromechanical models were created to understand the role of CNF in the composite foam boards. In addition to the theoretical modeling, practical investigation was performed to determine the nanomechanical properties of CNF using an Atomic Force Microscope (AFM) equipped with a Nanoindenter (NI).

This study resulted in successful development of eco-friendly composite foam boards that could be used for thermal insulation and packaging purposes. The nanomechanical properties of CNF were determined, the knowledge and information is a contribution to

our understanding of the role of CNF in composite structures. The results of this study show a significant opportunity for using CNF and the data on nanomechanical properties of CNF will provide crucial information to other researchers and industry experts who work on nanocellulose composites and on understanding the role of CNF in the composites.

ACKNOWLEDGEMENTS

I would like to express my appreciation to the many people at University of Maine who guided me through this research project. First and foremost, I thank Dr. Stephen M. Shaler for providing guidance, for the opportunity to work with him in many projects, and for valuable input to this research. The door to his office was always wide open whenever I had questions about my research or my life. He is much more than a thesis adviser and I am so thankful to him for steering me in this unique direction.

I would also like to thank Dr. Douglas Gardner for advice on understanding the behavior of raw materials, for use of his laboratory equipment, and for helping me adjust to a new culture. Dr. Robert Rice also deserves appreciation for our discussions on the investigation of the physical properties of nanocomposites and also for use of his laboratory equipment and his course on [*Wood Physics*]. I would also like to recognize Dr. Roberto Lopez-Anido for providing direction on understanding composite structures and Dr. Douglas Bousfield for providing advice on freeze-drying processes and understanding the behavior of mechanisms between corn starch and nanocellulose. I appreciate the help of Dr. Carl Tripp, who provided many important suggestions on the interaction of the raw materials used in this study.

I also owe a depth of gratitude to Russel Edgar (Sr. Lab. Operations & Wood Composites Manager), Jon Hill (Laboratory Engineering Specialist), and Chris West (Wood Plastic Composites Research Associate), who helped me to get used to working with the equipment at the Advanced Structures and Composites Center. I am so thankful to the University of Maine's School of Forest Resources Team including Cindy Pascal (Administrative Support Supervisor) and Shannon Field (Administrative Specialist) and

also Advanced Structures and Composites Center team including Kimberly-Mae-Mentus (Administrative Specialist), Marcy Smith (Program Associate), Diane Moseley (Accounting Support Specialist III), Josh Plourde (Manager of Communications and IT Coordinator), Walter Morris (Engineering Technician), Christopher Urquhart (Safety and Laboratory Operations Manager), Tom Drake (Network Specialist) and Jonathan Bubier (Network Specialist).

I am grateful to the University of Maine's Pulp and Paper Process Development Center team for supplying the raw materials and for allowing me to use their equipment and laboratories. I owe special thanks to Dr. David Neivandt and Mike Bilodeau, and to the entire staff and graduate students including Alexander Demers and Finley Richmond of the Chemical and Biological Engineering Department.

I am especially appreciative of the support I received from my home country, including a scholarship from The Republic of Turkey, Ministry of National Education, which allowed me to pursue my doctoral studies in the United States. I also acknowledge the McIntire-Stennis and United States Department of Agriculture, Agricultural Research Service for additional funding through my research.

And finally, I could not have successfully completed this thesis without the support of my family and I would like to dedicate my thesis to them. My parents and my brother always provided me their endless and sincere support whenever I need them. My wife and her unbelievable patience and support were crucial for this work. My two young daughters provided an abundance of happiness and motivation. I love you all!

TABLE OF CONTENTS

LIST OF TABLES

LIST OF FIGURES

CHAPTER 1

INTRODUCTION

1.1 Nanotechnology

Nanotechnology is research, investigation, and science performed at the nanoscale, where a nanometer is a unit equal to 1/25,400,000 of an inch. The diameter of a typical apple is roughly equal to 80 million nanometers (Figure 1.1). The popular physicist Richard Feynman is largely accepted as the father of nanotechnology. In 1959 Feynman famously asked "Why can't we write the entire 24 volumes of the Encyclopedia Britannica on the head of a pin?" (Feynman 1992). Since then, nanotechnology has been investigated and studied by many researchers and industry experts across the globe.

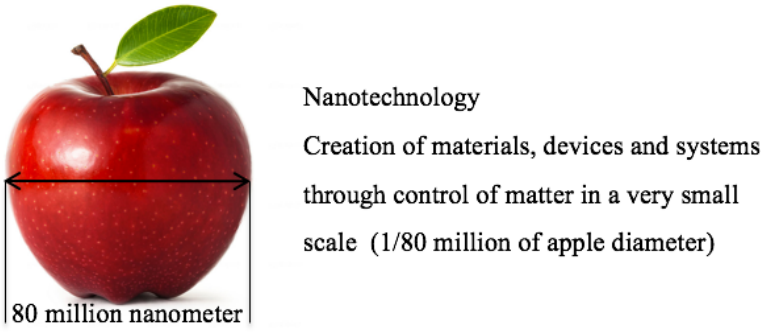

Figure 1.1: Demonstration of nanoscale.

The goal of nanotechnology is developing new materials or improving existing materials' properties through the features that can be obtained from the materials' nanostructures (Roco 2004). As Richard Feynman mentioned in his talk entitled "There's plenty of room at the bottom" (Feynman), materials have unique and impressive properties in their nanostructures.

Nanotechnology is a very important method of achieving the demands of today's society. People are looking for thinner computers, thinner screens, lighter smartphones, sensors that are not visible to human eye, super light guns, and similar countless needs that are all dependent on the improvements of nanotechnology. Nanotechnology has enabled the development or improvement of innovative products that have a dramatic influence on the economy and on our quality and standard of living. However, the most important thing that makes nanotechnology important is its interdisciplinary nature (Naschie 2006).

Nanotechnology can be applied in any area; however, research is most active in the fields of material science, applied physics, polymer science, and chemistry (Youtie and Porter 2009). Nanotechnology has been significantly used for creating new composite materials called nanocomposites.

1.2 Nanocomposites

Composites are materials created from two or more constituent materials where each has its own unique properties and, when they combined, a new material is created that has different characteristics than the individual starting materials. Nanocomposites follow the same principal where one or more phases has nanoscale dimensions embedded in a matrix.

There is a significant movement from using traditional materials such as metals and plastics to composite materials because composites exhibit desirable combinations of properties that aren't found in individual constituent materials (Ajayan and Tour 2007).

In the nanocomposite system there is a matrix, which is generally composed of metal, ceramic, or polymer. This matrix is reinforced using nanoparticles, nanofibrils, nanotubes, or nanolayering (nanoplates).

In this study, a polymer matrix, industrial corn starch, was reinforced with nanofibrils, specifically CNF. Microscopic images of the nanocomposites created and used in this study are shown in Figure 1.2.

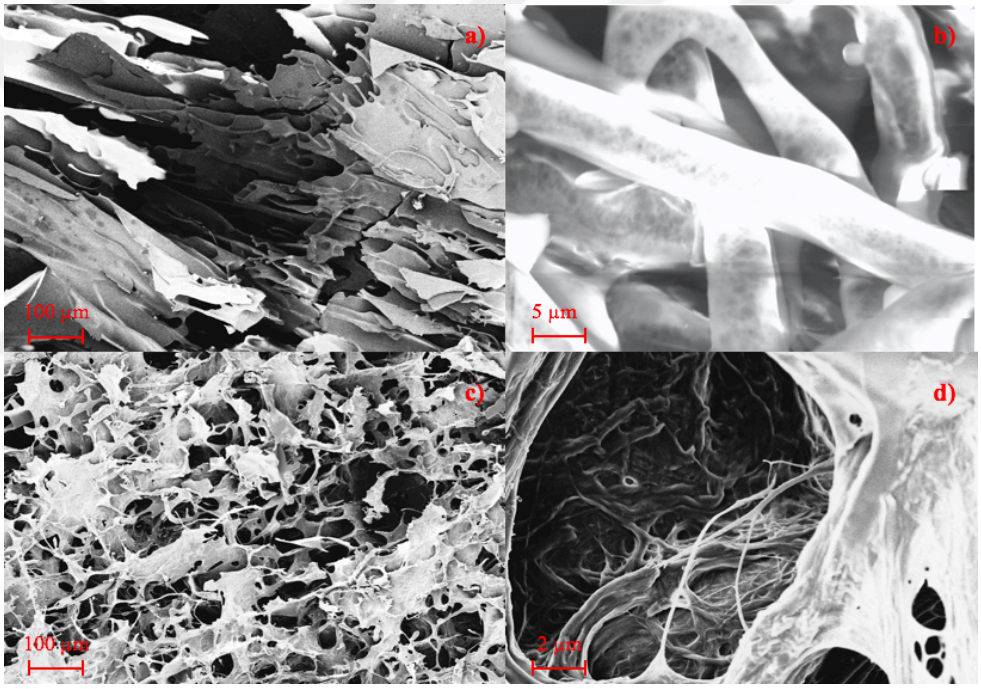

Figure 1.2: Demonstration of CNF-reinforced corn starch nanocomposite.
a) SEM images of freeze-dried cornstarch. b) Mechanically produced cellulose microfibrils and nanofibrils. c) CNF-reinforced corn starch composites. d) Corn starch cell walls embedded and reinforced with cellulose nanofibrils.

1.3 Cellulose nanofibrils (CNF)

Nanocelluloses have received attention in recent years and many researchers are studying its potential use as a raw material for a variety of products. One-third of the earth's land

area is covered by forests, making them a major component in the global ecosystem. The world's forests play significant role in climate change, habitat protection, the carbon cycle, water quality, and sustainable economies (Cai et al. 2013). About half of all major industrial cellulose, a raw material for chemical feedstocks, renewable energy, and nanocomposites, is derived from wood.

Nanocellulose can be categorized into three types: cellulose nanofibrils (CNFs), cellulose nanocrystals (CNCs), and bacterial celluloses (BCs) (Arvidsson et al. 2015). Nanocellulose can be produced by breaking wood down into nanometer-scale fibrils and particles and can be used for unique applications (Cai et al. 2013). In this study, the starting material was softwood CNFs (Figure 1.3), which also was named as nanobibrillated cellulose (NFC), microfibrillated cellulose (MFC) and cellulose microfibrils (CMF).

CNFs can be produced through different techniques including microfluidization, grinding, refining, high-intensity ultra-sonication (HIUS), cryo-crushing, or steam explosion (Sinke et al. 2016). CNFs used in this project were produced mechanically with no treatment, which has the lowest environmental impact (Nguyen 2014). However, the mechanical production of CNFs creates fibrils with a wide range of diameters, ranging from a couple of nanometers to several micrometers, as shown in Figure 1.3 (a,b,c and d).

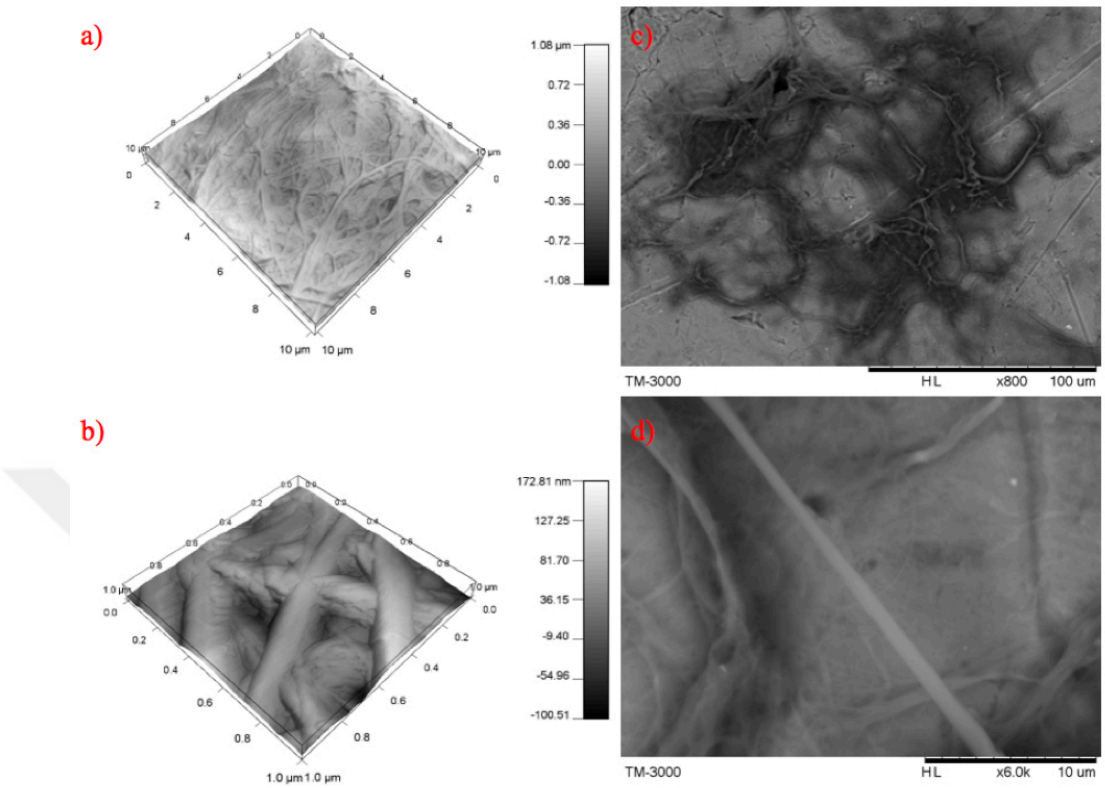

Figure 1.3: Representative Atomic Force Microscope (AFM) and Scanning Electron Microscope (SEM) images of CNFs.

a) AFM image of 100 µm2 scan area. b) AFM image of 1 µm2 scan area. c) SEM image of fibril distribution. d) SEM image of single microfibril and nanofibrils.

1.4 Corn Starch

The other major component of the nanocomposite produced in this study is corn starch, a readily available renewable resource that has many important industrial uses in films, foams, paper manufacturing, coatings, and variety of similar areas. On its own; however, corn starch is weak and brittle. When combined with CNF, the resulting material has excellent strength to weight properties, is very stable, and has excellent mechanical and thermal performance (Svagan et al. 2008).

Starch has two major components: (1) amylose consisting of α-(1-4)-linked D-glucose and (2) amylopectin consisting of a myriad α-(1-6)-linked branch point that needs to be cooked prior to final suspension because the crystal structure of the starch needs to be broken down to allow new bonds with the CNF. The main purpose of using industrial corn starch as a matrix material was to provide binding using hydrogen bonding and producing cross linking and to change the materials' physical structure from flexible to rigid.

1.5 CNF-based Nanocomposite Production Method and Embodied Energy Requirement

In this study, preliminary research was conducted to assess the "embodied energy" - the energy required for all of the processes associated with the production of a nanocomposite with the exception of starch production. The embodied energy includes the energy needed to produce the raw material, CNF, and also the energy needed to produce the nanocomposite from this raw material.

Figure 1.4 illustrates the total cumulative energy demand (CED) for CNF production. This study used mechanically produced CNFs, without treatment. Research (Arvidsson et al. 2015, Nguyen 2014) on investigating the environmental impacts of cradle-to-gate CNF production for different production routes are detailed below.

The enzymatic route:

1. Refining (Electricity)
2. Mixing pulp, enzyme, buffer (Enzyme and Buffer)
3. Incubation (Heat)

4.Mixing

5.Washing (Deionized water)

6.Enzyme denaturation (Heat)

7.Washing (Deionized water)

8.Refining (Electricity)

9.Adding microbiocide (Microbiocide)

10. Microfluidization (Electricity)

The no pretreatment route:

1.Homogenization (Electricity)

The caboxymethylation route:

1.Dispersion of pulp (Deionized water)

2.Washing and filtration (Ethanol)

3.Impregnation (Monochloroacetiacid, Isopropanol)

4.Carboxymethylation (Sodium hydroxide, Methanol, Heated isopropanol)

5.Washing and filtration (Deionized water, Aceticacid)

6.Impregnation (Sodium bicarbobate)

7.Washing and filtration (Deionized water)

8.Microfluidization (Electricity)

This study has shown that the energy required to produce CNFs from wood, including the interim kraft pulp product, is between 100 and 1800 megajoules per kilogram (MJ/kg), depending on the method and type of kraft pulp (i.e., bleached or unbleached sulfate) (Arvidsson et al. 2015, Nguyen 2014).

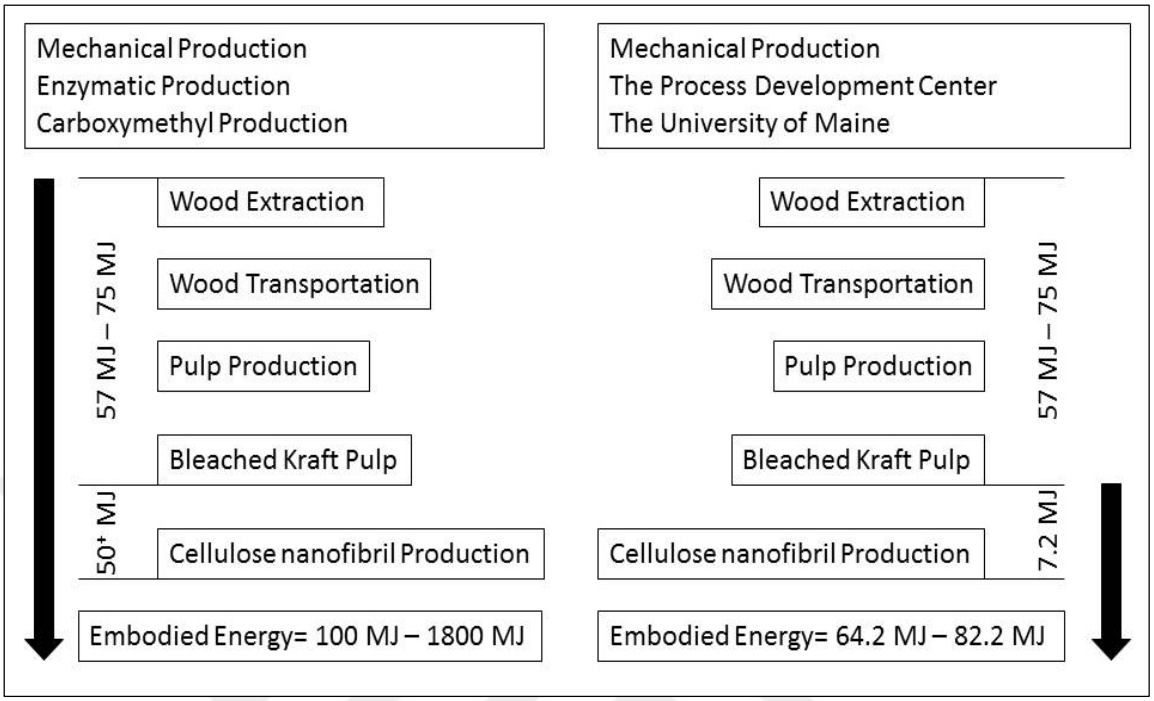

Figure 1.4: Total cumulative energy demand for CNF production.

Although the energy needed to produce the kraft pulp is dependent on others, the University of Maine's (UMaine's) Process Development Center has developed an advanced, low energy method for producing CNFs from kraft pulp. According to Michael Bilodeau, Director, energy required to produce CNFs from kraft pulp is 7.2 MJ/kg.

The second component of the embodied energy is production of the nanocomposite itself. In this study, cutting-edge freeze-drying technology (Figure 1.5) was used to produce the nanocomposite.

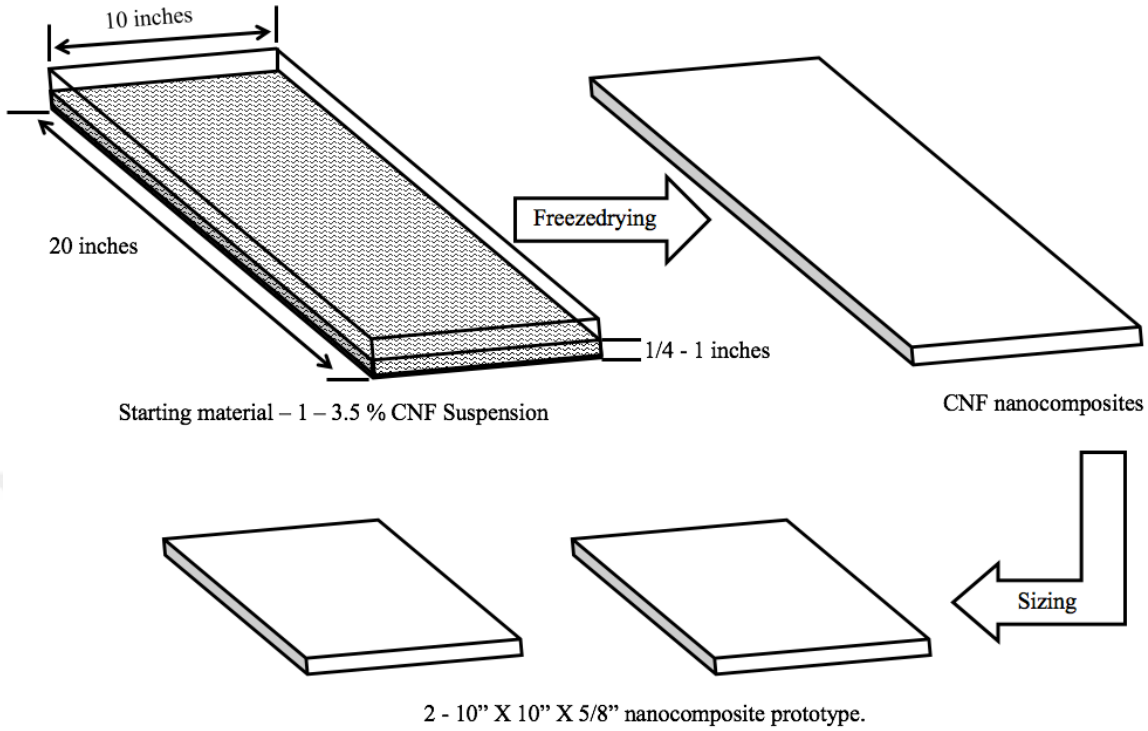

Figure 1.5: Representation of nanocomposite production process.

The freeze-drying process was performed between 20 ºC and -45 ºC and at pressures of between 100 and 0.01 mbar. As shown in Figure 1.6, the freeze-drying process included different phase changes, each with its own energy inputs according to the phase change type (e.g., liquid to solid or solid to gas). Specific heat values (c), heat of vaporization (hv), heat of fusion (hf), and heat of sublimation (hs) were used to calculate nanocomposite production energy. Based on specialized production process and detailed energy calculations, the energy required for producing nanocomposite from CNF is estimated to be between 4 and 8 MJ/square foot (sf) for 5/8" thickness.

The total required energy was calculated determining the required energy for each temperature change and each phase change. For calculating the required energy for

temperature changes, the equation 1.1 was used and for the phase changes equation 1.2 and equation 1.3 was used according to occurred phase change.

$$q = m \times c \times \Delta T \quad \text{(Eq. 1.1)}$$

where;

q = heat energy gained or lost by a substance (J)

m= mass (kg)

c = specific heat (J/g°C)

c_{water} = 4.187 (J/ g°C)

c_{ice} = 2.108 (J/ g°C)

c_{vapor} = 1.996 (J/ g°C)

ΔT = change in temperature (°C)

$$q = m \times H_f \quad \text{(Eq. 1.2)}$$

where;

H_f = heat of fusion (333.55 (kJ/kg))

$$q = m \times H_v \quad \text{(Eq. 1.3)}$$

where;

H_v = heat of vaporization (2260 (kJ/kg))

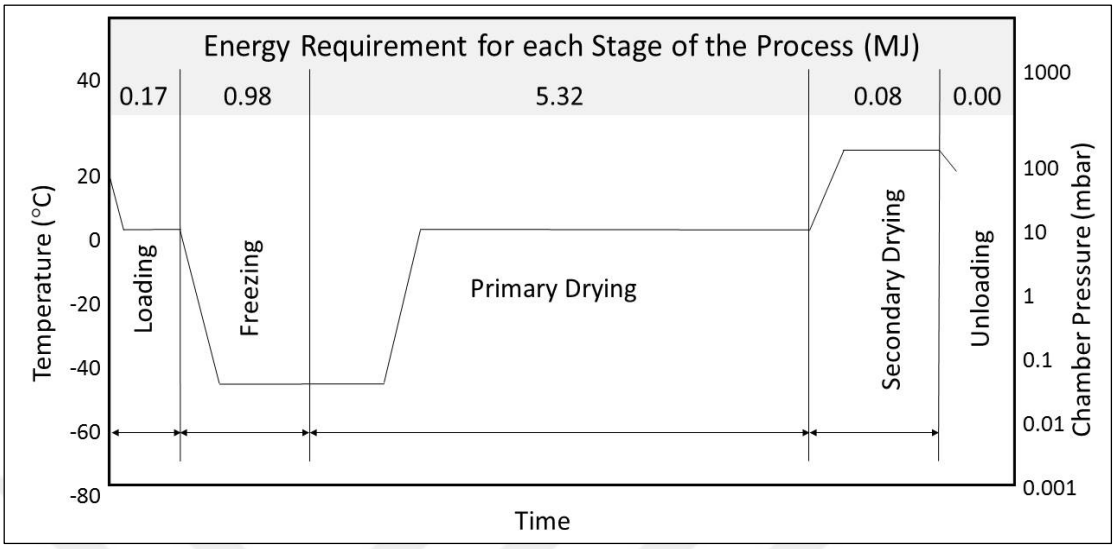

Figure 1.6: Freeze-drying process and energy requirements by phase change.

Adding the energy required for CNF production to the energy estimated for nanocomposite production process, the total embodied energy is estimated to be between 6 and 10 MJ/sf for 5/8" thick material.

1.6 Thesis Objectives

The overall goal of this thesis was to assess the usefulness of nanocellulose-based composite materials in new products, especially for rigid foam boards for insulation, packaging, and similar purposes. Using green and eco-friendly materials, these new products will increase the producer's and user's safety, reduce the amount of inorganic waste, reduce carbon emissions in the production process and use of foam boards, and provide for a cleaner environment. The goal of the research was to produce foam boards with mechanical and thermal properties comparable to or better than typical petroleum-based polystyrene foam boards, but with a dramatically lower carbon footprint.

Specific objectives for this thesis include the following:

Developing a process for producing innovative foam boards using organic polymers: corn starch and cellulose nanofibrils. In this objective, the nanocomposite production method (freeze-drying) that we used allowed the production of panels from an aqueous suspension of CNF and corn starch solution. The required steps and parameters (temperature, time, pressure and etc.) were determined.

To understand the mechanisms and interactions between the corn starch and the CNF. Corn starch and CNF both are hydrophilic polymers (i.e., they easily attract water) with many hydroxyl (OH) groups in their structure. However, bonding needs to be created homogeneously and in this step the interactions of CNF and corn starch were studied and the conditions for the optimum interaction were determined.

To understand the mechanisms, optimum corn starch and CNF ratio, and the amount of solid contents (% by weight) that provides the desired mechanical, thermal, and physical properties. In this objective, the optimum starch solution and CNF suspension concentration and also the optimum ratio between the starch and CNF were determined to reach the desired material properties.

To determine the potential of using CNF as a reinforcing material and the role of CNF in nanocomposites. There is a significant lack of knowledge of the nanomechanical properties of CNF, creating a problem for researchers and industry experts to understand the role of CNF in the nanocomposite structures. Additionally, lack of nanomechanical information is an impediment for theoretical calculations and

predictions of CNF's nanomechanical properties. In this objective, the nanomechanical properties of CNF and its role in the nanocomposites were investigated and determined.

1.7 Thesis Format

This thesis is written as a combination of separate publications or potential publications in chapter format; therefore, some of the background material and literature review may be repeated in the chapters. Following is an outline of this thesis, including the publications:

Chapter 1. Introduction

Chapter 2. Production (A combination of three publications)

Yildirim N., Shaler S.M., Gardner D.J., Bousfield D.W. and Rice R. (2013), Cellulose Nanofibril (CNF) Insulating Foams, Contributing Author, Production and Applications of Cellulose Nanomaterial, Author: Michael T. Postek, Robert J. Moon, Alan W. Rudie, Michael A. Bilodeau, ISBN: 978-1-59510-224-9.

Yildirim N., Shaler S. M., Gardner D.J., Bousfield D.W. and Rice R. (2014), Cellulose Nanofibril (CNF) Reinforced Starch Insulating Foams, Cellulose, 21 (6): 4337-4347.

Yildirim N., Shaler S.M., Gardner D.J., Rice R. and Bousfield D.W. (2014), Cellulose Nanofibril (CNF) Reinforced Starch Insulating Foams. MRS Proceedings, (1621); 177-189.

Chapter 3. Theoretical Calculations and Predictions

Shaler S.M., Lopez-Anido R. and Yildirim N. (2014), Cellulose Nanofibril (CNF) Reinforced Open Cell Foams; Application of Cubic Array Foam Theory, 57th SWST International Convention, Technical University in Zvolen, Zvolen, Slovakia, June 23-27 pp 451-458.

Chapter 4. Understanding the Actual Role of Cellulose Nanofibrils in Nanocomposites

Yildirim N. and Shaler S.M. (2015), Nanomechanical properties of cellulose nanofibrils (CNF), "MRS Advances", DOI: http://dx.doi.org/10.1557/adv.2015.30, 2015.

Chapter 5. The Application of Nanoindentation For Determination of Cellulose Nanofibrils (CNF) Nanomechanical Properties

Yildirim N. and Shaler S.M. (2016), Investigation of cellulose nanofibrils's (CNF) behavior under nano forces through different approaches. Under Review.

Chapter 6. Conclusions and Recommendations

CHAPTER 2

CELLULOSE NANOFIBRIL (CNF) REINFORCED STARCH INSULATING FOAMS

2.1 Abstract

In this study, biodegradable foams were produced using cellulose nanofibrils (CNFs) and starch (S). The availability of high volumes of CNFs at lower costs is rapidly progressing with advances in pilot-scale and commercial facilities. The foams were produced using a freeze-drying process with CNF/S water suspensions ranging from 1 to 7.5 % solids by weight. Microscopic evaluation showed that the foams have a microcellular structure and that the foam walls are covered with CNF`s. The CNF's had diameters ranging from 30 nm to 100 nm. Pore sizes within the foam walls ranged from 20 nm to 100 nm. The materials' densities ranged from 0.012 to 0.082 g/cm3 with corresponding porosities between 93.46% and 99.10%. Thermal conductivity ranged from 0.041 to 0.054 W/m-K. The mechanical performance of the foams produced from the starch control was extremely low and the material was very friable. The addition of CNF's to starch was required to produce foams which exhibited structural integrity. The mechanical properties of materials were positively correlated with solids content and CNF/S ratios. The mechanical and thermal properties for the foams produced in this study appear promising for applications such as insulation and packaging.

2.2 Introduction

In recent years, there has been increasing interest in development of nanocomposites based on nanocellulosic materials (Siro and Plackett 2010). In this study cellulose nanofibril and starch insulation foams were produced and characterized. The main reason

for using cellulose is that it is an abundant material, which can be obtained from renewable sources including a broad range of plants and sea animals (Moon et al. 2010). Starch is another abundant natural polymer, which is a promising raw material for the development of novel materials (Martins et al. 2009). It is a widely available biopolymer with a price half that of polyethylene and polystyrene. Annually, millions of metric tons of starch are used as non-food products in the paper and textile industries (Glenn et al. 2011). Starch is mostly water soluble, difficult to process and has low mechanical properties. It was found that reinforcing starch with cellulose microfibrils increases the mechanical properties significantly (Dufresne and Vignon 1998). Glenn and Irving produced microcellular starch foams with different drying techniques and investigated the mechanical and thermal properties. They showed that mechanical properties of microcellular foams are positively correlated with density. They found that corn starch foams exhibited greater compressive strength (0.19 -1.14 MPa) and density (0.12-0.31 g/cm3) than the wheat starch and high amylose cornstarch foams. (Tatarka and Cunningham 1996) showed most starch-based foams have similar compressive strength (0.0927 MPa) with EPS foams. (Chen et al. 2004) studied starch graft poly (methyl acrylate) loose-fill foams and they found that starch graft poly (methyl acrylate) foams (S-g-PMA foams) have 0.07±0.01 MPa compressive strength with 0.0086±0.00021 g/cm3 density. (Nabar et al 2005) showed that starch based foams have compressive strengths of between 12.5 and 13.1 Pa with the densities changes from 0.003 to 0.0035 g/cm3. (Svagan et. al. 2011) investigated the mechanical properties of amylopectin-based foams with varying microfibrillated cellulose (MFC) contents and they showed increasing the MFC content produces higher mechanical properties, however,

maximizing the MFC content doesn't mean having the highest mechanical properties. (Svagan et. al. 2008) obtained the optimum mechanical properties from the 40% MFC reinforced foams when compared to 0%, 10% and 70% MFC reinforcements. On the other hand, (Glenn et al. 2007) found that, adding soft wood fibers to starch foams increases the thermal degradation temperature from 270 °C to over 300 °C. Dispersed cellulose fibers significantly increase the mechanical and thermal properties of starch foams as shown by (Glenn and Irving 1995) who produced corn starch foams have thermal conductivity values ranging from 0.037-0.040 W/m-K.

The higher specific properties of cellulose nanofibrils (CNF) compared to the previously used forms of wood reinforcement was judged to offer an opportunity for additional improvements. This exploratory study aimed to determine the impact of solids content and CNF/S ratio on the morphology, physical, and mechanical properties of insulation foams with the intent to evaluate their suitability for application as structural insulation foam or other market opportunities.

2.3 Materials and Methods

Cellulose nanofibrils (CNF) used in this study was produced by the University of Maine Process Development Center. The CNF was prepared mechanically using a pilot-scale double disk refiner to fibrillate a bleached softwood Kraft pulp. The materials are typically 20-50 nm in diameter and have a length of several micrometers. Five different thermal insulation foams were prepared from aqueous suspensions (tap water + material) with the following solid contents: 1% CNF, 0.5% CNF+0.5% starch, 1.5% CNF+3% starch, 1.5% CNF+6% starch and 7.5% starch (Table 2.1).

Table 2.1: Experimental design of produced foams.

Sample	Number of Samples (30.6 cm x 61 cm x 3.5 cm)
0.5% CNF+ 0.5%Starch	4
1% CNF	4
1.5% CNF+ 3%Starch	4
1.5% CNF+ 6%Starch	4
7.5% Starch	4

The CNF/water suspensions were obtained at 3% solids by weight. The CNF suspensions were reduced to 1 5 solids by weight by adding water into the suspension. The suspension was placed in a 20 L capacity container. A high shear mixer was used to disperse the CNF in suspension (1700 RPM for 20 minutes). For creating the starch foams, industrial corn starch (Tate&Lyle) was used and cooked at 87.8 °C (190 °F) and mixed at 500 RPM for one hour. Starch solutions were cooled down to the room temperature (23±2°C). The final solids content was determined by oven drying 30 to 35 grams suspension samples. The suspensions had a high consistency and were gel-like in appearance. Starch solution and CNF suspension were put into high shear mixer and dispersed (1700 RPM for 20 minutes). The dispersed suspensions were poured into trays (30.6 cm x 61 cm) to a depth of 3.5 cm and placed in a freeze dryer. Suspensions were freeze-dried using a Millrock Technology Max53 freeze dryer utilizing the Opti-Dry 2009 control system. T-type thermocouples were placed in the material to monitor temperature during the freeze-drying process. At first, partial vacuum was pulled then he chamber temperature was lowered from 20 °C to -45°C in 1 hour and maintained at that temperature for 250 minutes. The chamber was then evacuated to a pressure of 100 mTorr. The chamber temperature was maintained at -45°C for 30 minutes, ramped to 0˚C over 2 hours, ramped to 20°C in 4 hours and then maintained until average thermocouple reading in the

materials was 20°C for 4 hours, which was the proof of completed freeze drying obtained through multiple preliminary drying.

2.4 Morphology

Representative CNF/starch foam samples were imaged using scanning electron microscopy (SEM) and atomic force microscopy (AFM). For the SEM measurements, 3 mm x 3 mm x 2 mm samples were prepared from the freeze dried foams using a razor blade, placed on double-sided carbon paper and pasted onto stubs. SEM micrographs were obtained with a Zeiss Nvision 40 FIB-SEM at an acceleration voltage of 5.0 kV after gold-palladium (Au:Pd) sputter coating (~ 15 nm thickness) was applied to the specimens. Surface topography was measured with an MFP-3D AFM (Asylum Research). Specimens (foam powders) were pasted onto stubs using an epoxy adhesive and imaged 24 hours later. Images were obtained a chamber temperature of 25 °C using tapping mode (AC Mode) and an Asylum Research AC240TS-10 cantilever tip with a 9±2 nm radius with spring constant, k (N/m) =2 (0.5-4.4).

2.5 Physical Properties

The following subsections present the physical properties of the CNF/starch foam samples.

2.5.1 Density & Relative Density

Density measurements of the foams were performed according to ASTM C303-10 by measuring six 150 mm x 150 mm x 25.4 mm (6 in x 6 in x 1 in) specimens from each group. The measured mass (g) was divided by the measured volume (cm3) to calculate the density. Relative density is a significant property for the cellular materials which is

the ratio between bulk density (Pbulk) and particle density (Pparticle) (Gibson and Ashby 1998).

2.5.2 Porosity

The void fraction, which is called porosity, the ratio of pore volume to its total volume of foams, was calculated using liquid porosimetry method (Gibson and Ashby (1998)) (Equation 2.1.).

$$\phi = 100x\left(1-\frac{\rho_{bulk}}{\rho_{particle}}\right) \quad \text{(Eq. 2.1)}$$

where;

ϕ = Porosity

P_{bulk} = Density of the foam

$\rho_{particle}$ = Density of the beams & columns (CNF + CS, 1.50 g/cm3)

Volume Fractions

Fiber volume fraction which is the volume fraction of the fibers in the composition is calculated using equation 2.2. (Reuss 1929).

$$V_f = \left(\frac{\text{Volume of Fibers}}{\text{Volume of Fibers} + \text{Volume of Matrix}}\right) \quad \text{(Eq. 2.2)}$$

where;

V_f= Fiber volume fraction

2.6 Mechanical Properties

Results of flexural and compression testing of the CNF/starch foam samples are presented in the following subsections.

2.6.1 Flexural Testing

Six (6) samples with 300 mm x 100 mm x 25.4 mm (12 in x 4 in x 1 in) dimensions from each sample group were tested by using a three-point bending test method according to ASTM C203-12. The crosshead displacement rate was 6 mm per minute. Specimen displacement was obtained from the crosshead displacement (Instron 5966, with 100KN maximum load). Flexural tests were applied under laboratory conditions (25±2 °C and 50% relative humidity). The flexural modulus of the foams was obtained from the linear initial part of the force-deflection curves (Figure 2.1).

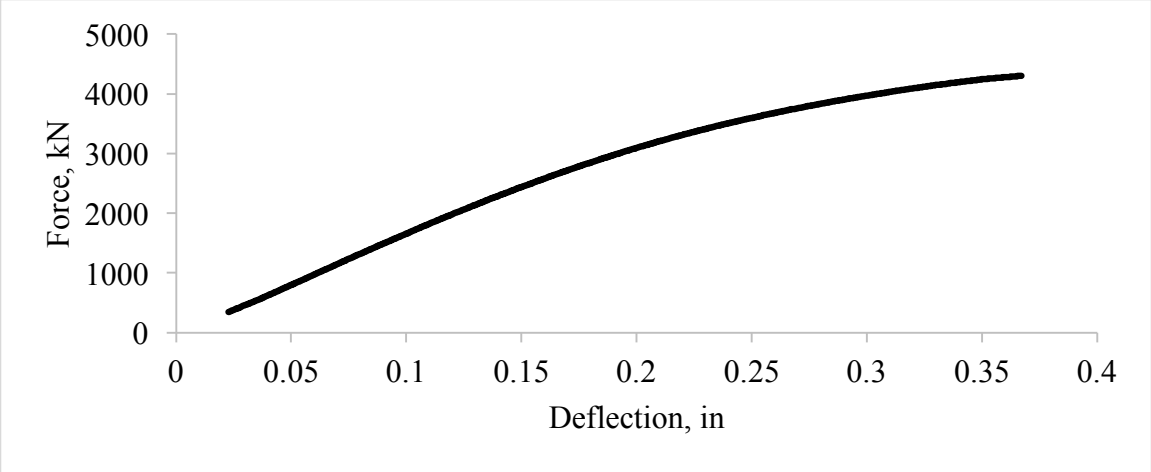

Figure 2.1: Typical force-deflection curve for flexural tests of foams (1.5 % CNF + 6 % CS).

2.6.2 Compression Testing

Six (6) samples with 150 mm x 150 mm x 25.4 mm (6 in x 6 in x 1 in) dimensions from each sample group were tested according to ASTM C165-07. Each specimen was compressed at a rate of 6 mm per minute and the specimen displacement was obtained from the crosshead displacement (Instron 5966, with 100kN maximum load). Compression tests were conducted under laboratory conditions, 25±2 °C temperature and

50% relative humidity and the specimens were conditioned for one day prior to testing. The compression modulus was obtained from the linear initial part of the force-deflection curves (Figure 2.2).

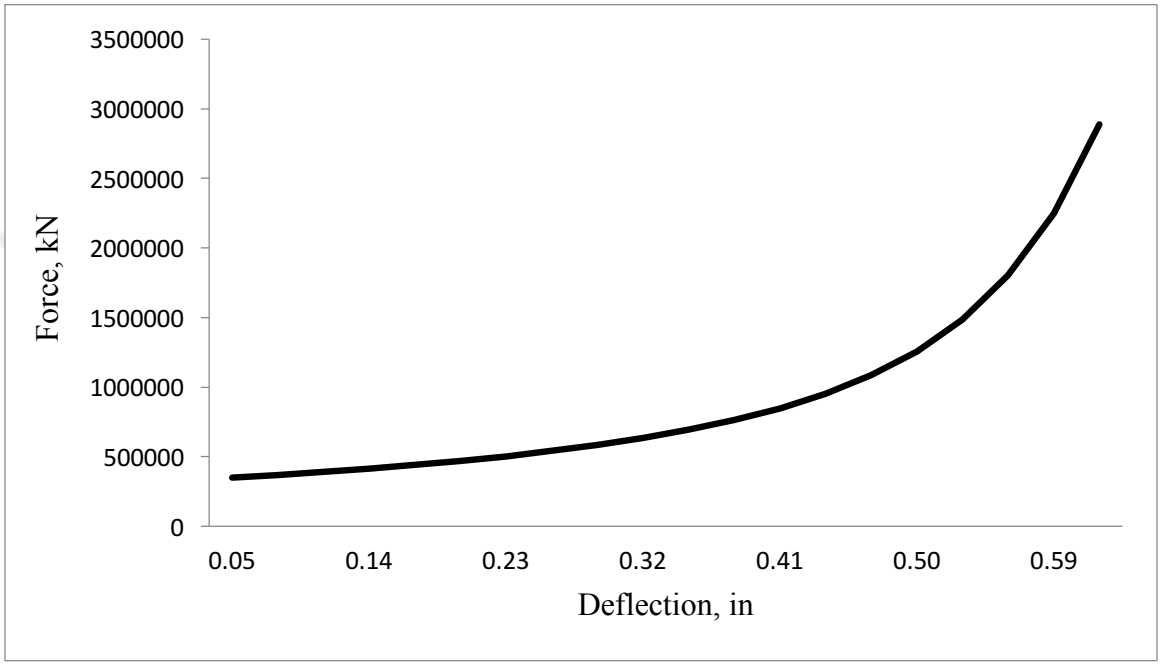

Figure 2.2: Typical force-deflection curve for compression tests of foams. (1.5 % CNF + 6 % CS).

2.7 Thermal Properties

Results of testing the CNF/starch foam samples for thermal properties are presented in the following subsections.

2.7.1 Thermal Conductivity Measurements

Six (6) specimens (300 mm x 300 mm x 25.4 mm) were prepared from each group, two specimens from each tray. The steady-state thermal transmission was measured according to ASTM C518-10 using a heat flow meter (NETZSCH Lambda 2000 heat flow meter).

2.7.2 Thermogravimetric Analysis (TGA)

Six (6) specimens from each group, which weighed from 6 g to 10 g, were prepared as a powder and placed into crucibles according to ASTM E113-08. The thermogravimetric analysis was conducted from 25 °C to 800 °C with 10 °C increase per minute using a Mettler Toledo Thermogravimetric Analyzer (TGA/SDTA851e).

2.8 Statistical Analysis

The density, compression, flexure strength and modulus, thermal conductivity, thermal resistivity, and thermogravimetric analysis data were compared by conducting a one-way Means/ANOVA to check if there was a significant overall difference (significance level (alpha) = 0.01). Significant differences between groups were evaluated by use of a Tukey-Kramer Honestly Significant Differences (HSD) test with alpha=0.05. A sample size of six (n=6) was used for all statistical analysis.

2.9 Results and Discussion

The large range in sample density (0.013 to 0.098 g/cm^3) resulted in all statistical analysis having significant overall differences. There was a significant effect of solids content on the porosity, density and relative density (Table 2.2). As expected, including less solids content in the suspension produced a more porous structure. The reason for the inverse proportion between solid content and porosity can be explained by the increased bonds with increase solid content between starch and CNF in the same volume. This indicates that the production process (suspension-dispersion) and foam preparation method (freeze-drying) can be manipulated to produce foams of varying density and porosity.

Table 2.2: Physical properties of foams.

Sample	Solid-Water Content	Fiber Volume fraction (%)	Density (g/cm3)	Relative Density	Porosity (%)
0.5% CNF + 0.5% Starch	1%-99%	50	0.013 (7.6) D	0.00867	99.10 (0.1) A
1% CNF	1%-99%	100	0.014 (11) D	0.00933	99.10 (0.1) A
1.5% CNF + 3% Starch	4.5%-95.5%	33.3	0.053 (2.1) C	0.03533	96.50 (0.1) B
1.5% CNF + 6% Starch	7.5%-92.5%	20	0.076 (2.6) B	0.05067	94.95 (0.1) C
7.5% Starch	7.5 %-92.5%	0	0.098 (3.7) A	0.06533	93.46 (0.1) D

Note: Parentheses indicate the coefficient of variation (COV, %). A, B, C and D letters indicates the significant differences between the treatments.

A representative set of SEM images and fiber size measurements of the foams are given in Figure 2.3. It is shown that there is variety in fibril diameters attributable to production process (shear mixing + freeze-drying) where the fibrils were individually and randomly resized, and also individually freeze dried, and raw material (mechanically produced CNF). The selected fibrils show the average fibril diameters, whereas there are fibrils with couple hundred nanometers diameters and there are other fibrils with less than 10 nanometers diameters in the structure as well. Some damage (cracking) was evident because of sample preparation process (razor blade cutting). The structure of the foam wall material was evaluated (Figure 2.3b). The foam wall structure is a plate of CNF material embedded within a starch matrix. Further investigation of the foam cell wall material (Figure 2.3c) illustrates the nanoscale fibril structure of the CNF with diameters ranging mostly from 30 to 100 nanometers.

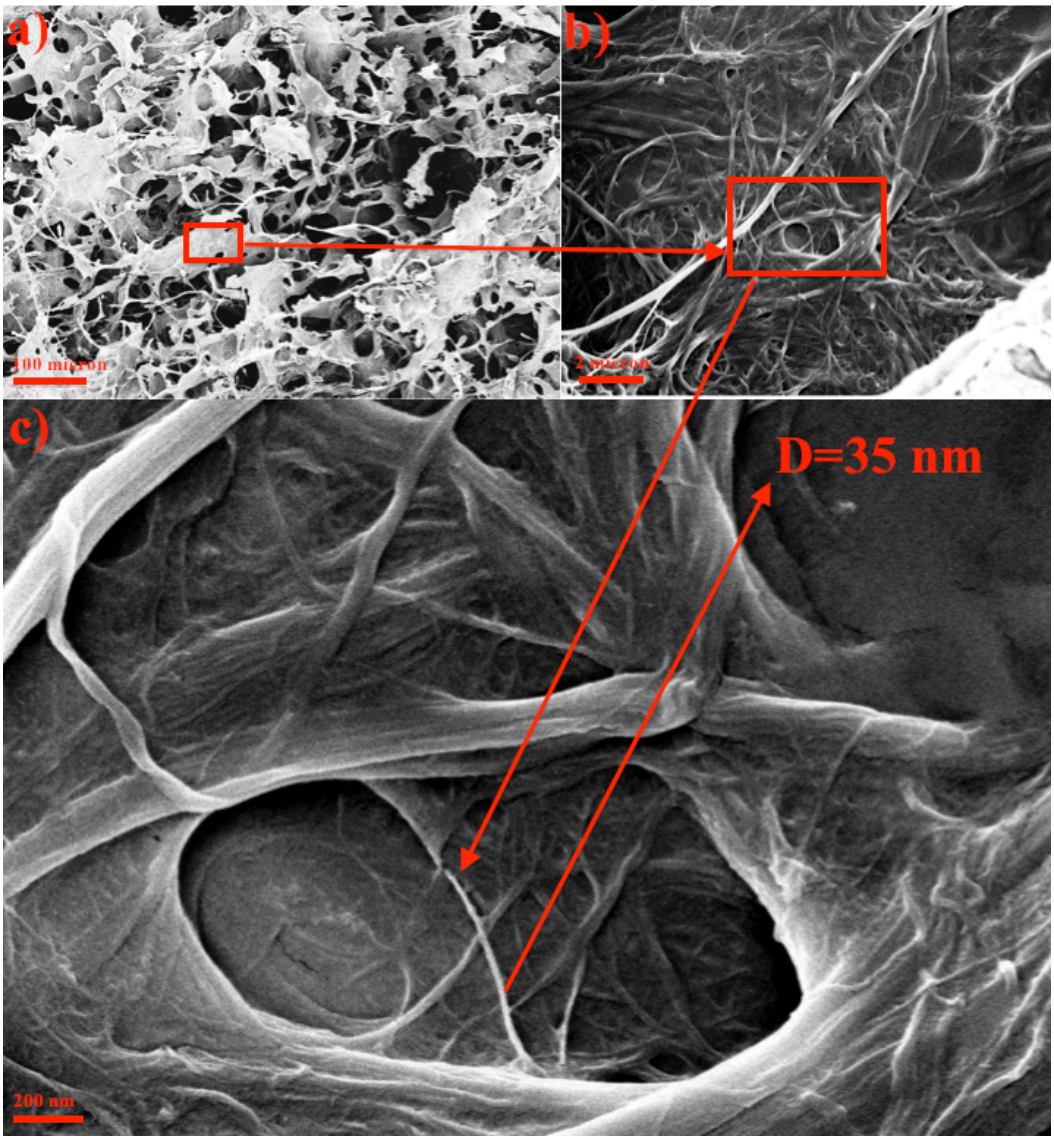

Figure 2.3: Representative SEM images of foams (1.5% CNF + 6% S).

(a) Cellular structure. (b) Distribution of nanofibrils in 2 micron scale bar. (c) Fibril diameter measurements.

Atomic force microscopy (AFM) was used to measure the diameter of nano pores in the cellular wall material. It was determined that the diameter of the pores (Figure 2.4) ranged from 20 nm to 100 nm. The difference between the SEM and AFM images can be

explained by the difference in imaging principles and different regions and field of view of the images.

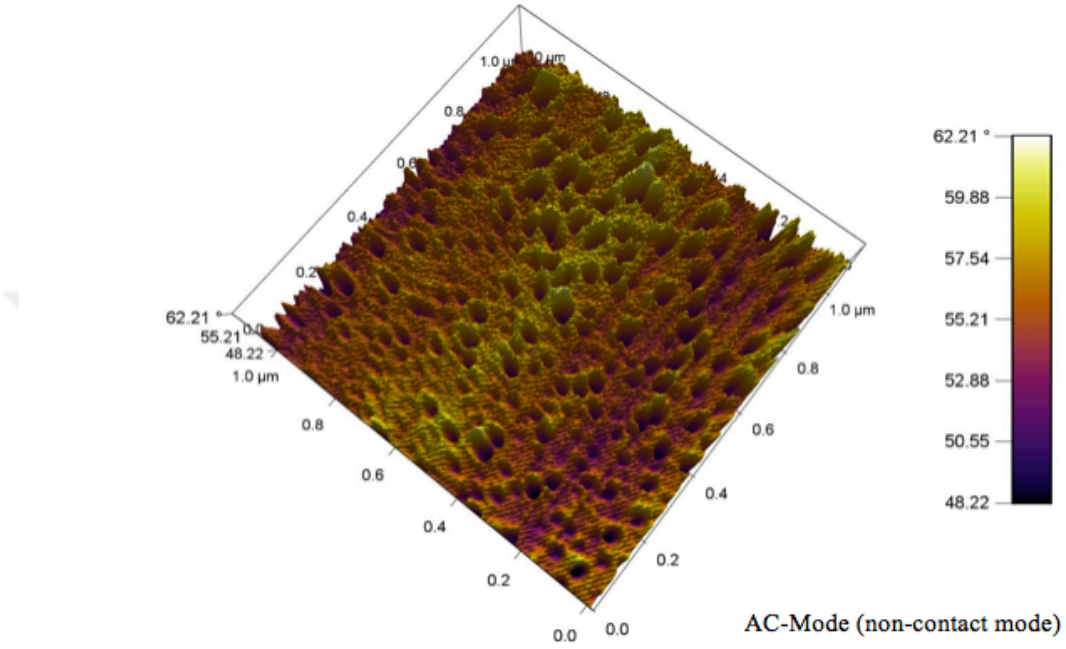

Figure 2.4: Representative AFM images of foams (1.5% CNF + 6% S).

The density, flexural modulus and flexural strength (MOR) of the foams are summarized in Table 2.3. Density of the foams ranged between 0.013 to 0.082 g/cm3. The increase in the solids content increased the total mass of the foam structure, which increased the density. The elastic modulus (MOE) and modulus of rupture (MOR) plotted against density are shown in Figure 2.5.

Increasing the density was correlated with increases in modulus of elasticity (MOE) and modulus of rupture (MOR) and a curvilinear relationship was indicated between density and flexural properties. However, pure starch foams with even higher solid content (7.5%) and density exhibited very low mechanical properties.

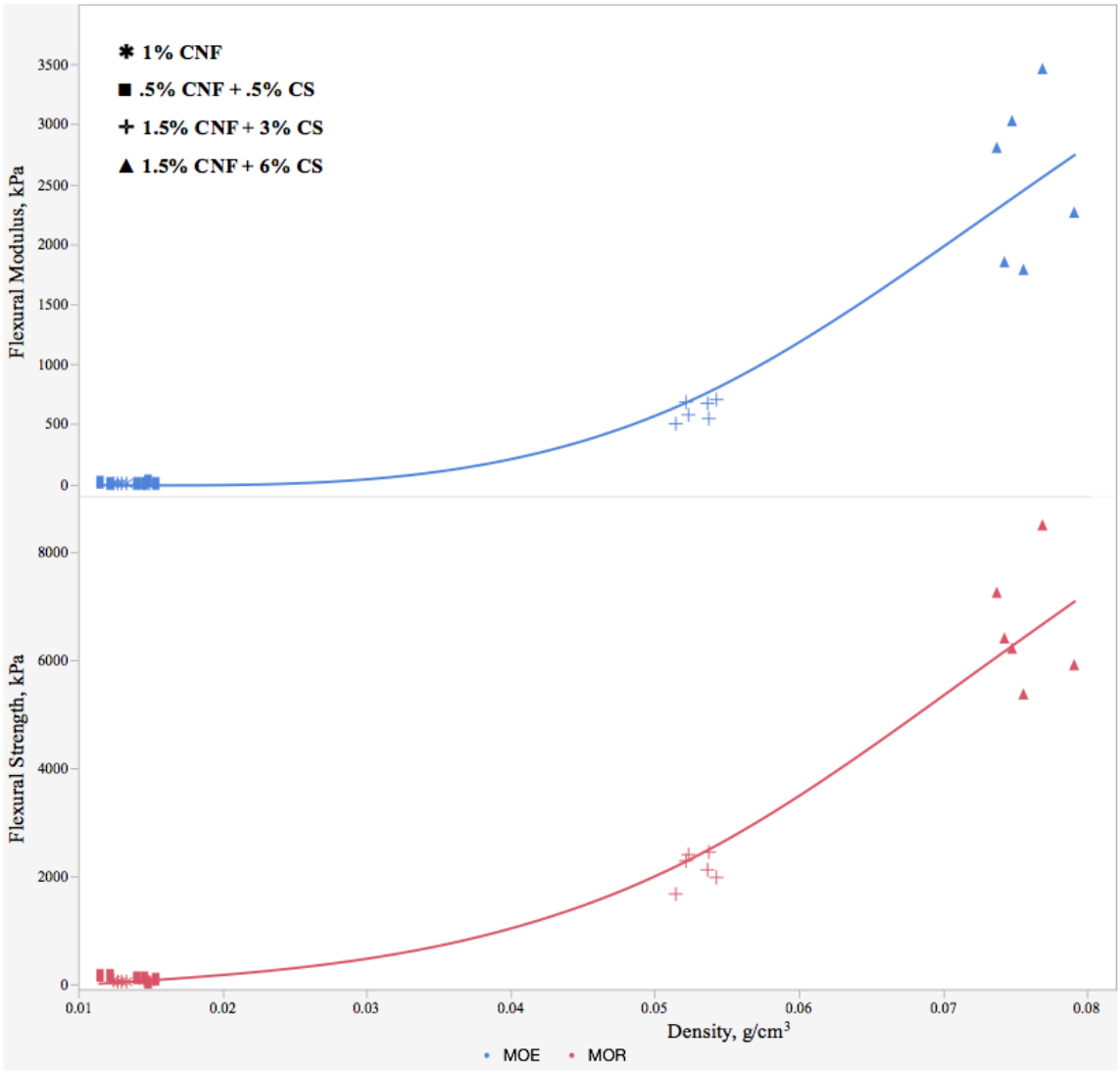

Figure 2.5: The flexural modulus and flexural strength of foams plotted against density.

Reinforcement of the starch foams using CNF produced significant increases in flexural properties for all groups. However, when the 1% CNF (blue sign in Figure 2.5) and 0.5% CNF + 0.5% S (yellow sign in Figure 2.5) combinations were compared, it seems there is no effect of adding CNF because of the given scale in "y" direction. The CNF addition produced an 84% increase in MOE and 71% increase in MOR (Table 2.3). In addition to this, when 3% starch or 6% starch was reinforced with 1.5% cellulose nanofibrils, flexural properties increased significantly.

Table 2.3: Flexural properties of foams.

Sample	Density (g/cm3)	Elastic Modulus (kPa)	Modulus of Rupture (kPa)
0.5% CNF + .5%Starch	0.013 (5.0) D	2.30 (48) C	40.00 (25) C
1% CNF	0.014 (8.6) D	14.0 (60) C	140.0 (29) C
1.5% CNF + 3%Starch	0.053 (2.1) C	610 (13) B	2140 (14) B
1.5% CNF + 6%Starch	0.082 (5.9) B	2530 (26) A	6590 (17) A
7.5% Starch	0.098 (3.6) A	N/A	N/A

Note: Parentheses indicate the coefficient of variation (COV, %). A, B, C and D letters indicates the significant differences between the treatments. The extreme friability of the 7.5% starch specimens did not allow for determination of the mechanical performance.

As detailed in Table 2.3. high coefficient of variations were found in flexural properties, especially for elastic modulus results. The force deflection curves were investigated and compared in one chart as given in Figure 2.6.

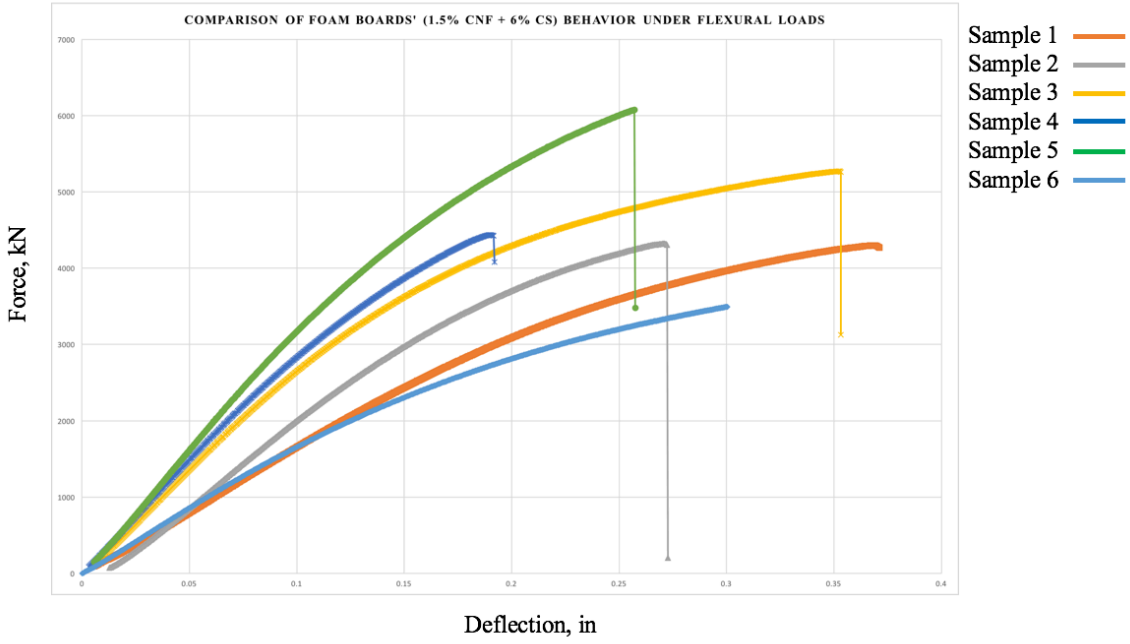

Figure 2.6: The comparison of foam boards' behavior under flexural loads.

As it is shown in Figure 2.6, each sample has different response to applied load, which can be related with their material structure. The main reason behind this difference so the high coefficient variations can be explained as followed.

Micro/nano cellular structure; the developed structure has voids and the diameters, shape of the voids varies as shown in Figure 2.3., each void and its shape, diameter effects the behavior of the representative region under forces. High variety of the voids geometrical differences and the amount of total voids in each sample has a significant role in these high COVs.

Heteregenous production and reinforcement; Also, as shown in Figure 2.3., CNF reinforces CS in the cellular structure. Each beam and column that connects each unit to another, transfers the stress in this structure. Due to production process (freeze drying) limitations, the reinforcement occurs naturally and each beam and column can be reinforced in a different way and amount. As a result of the production limitation and random reinforcement high COVs can be expected.

Studies have indicated that the commercial polystyrene structural foam (Styrofoam™) has a 1610 kPa stress at yield (Shey et al. 2006). Gypsum board has 4600 kPa modulus of rupture in the machine direction and 1500 kPa modulus of rupture in cross direction (Gypsum Association 2010). The performance of the 1.5% CNF/6% starch formulation exceeded both levels of performance.

The compression performance of the foams (Table 2.4) showed a trend consistent with that found for flexural behavior. Density was positively correlated with compression

modulus, compressive resistance and the maximum force when the specimens were compressed to 10% of specimen thickness (Figure 2.7).

The role of starch and CNF was directly evaluated at 1% solids content (1% CNF vs. 0.5% CNF + 0.5% Starch). The foam made with half starch resulted in significant decreases in compression modulus (50%), compressive resistance (60%) and maximum force (59%). For a constant solids content (1.5%) of CNF, increasing the starch content in the structure from 3% to 6% increase the compression modulus (83%), compressive resistance (21%), and maximum force (148%).

It was also found that, at low density, addition of corn starch decreases the mechanical performance whereas at higher densities (0.053 g/cm^3 – 0.076 g/cm^3) the addition of corn starch produces higher compression performance. This could be related with the amount of corn starch needs to be used relative to CNF amount for cross linking purposes.

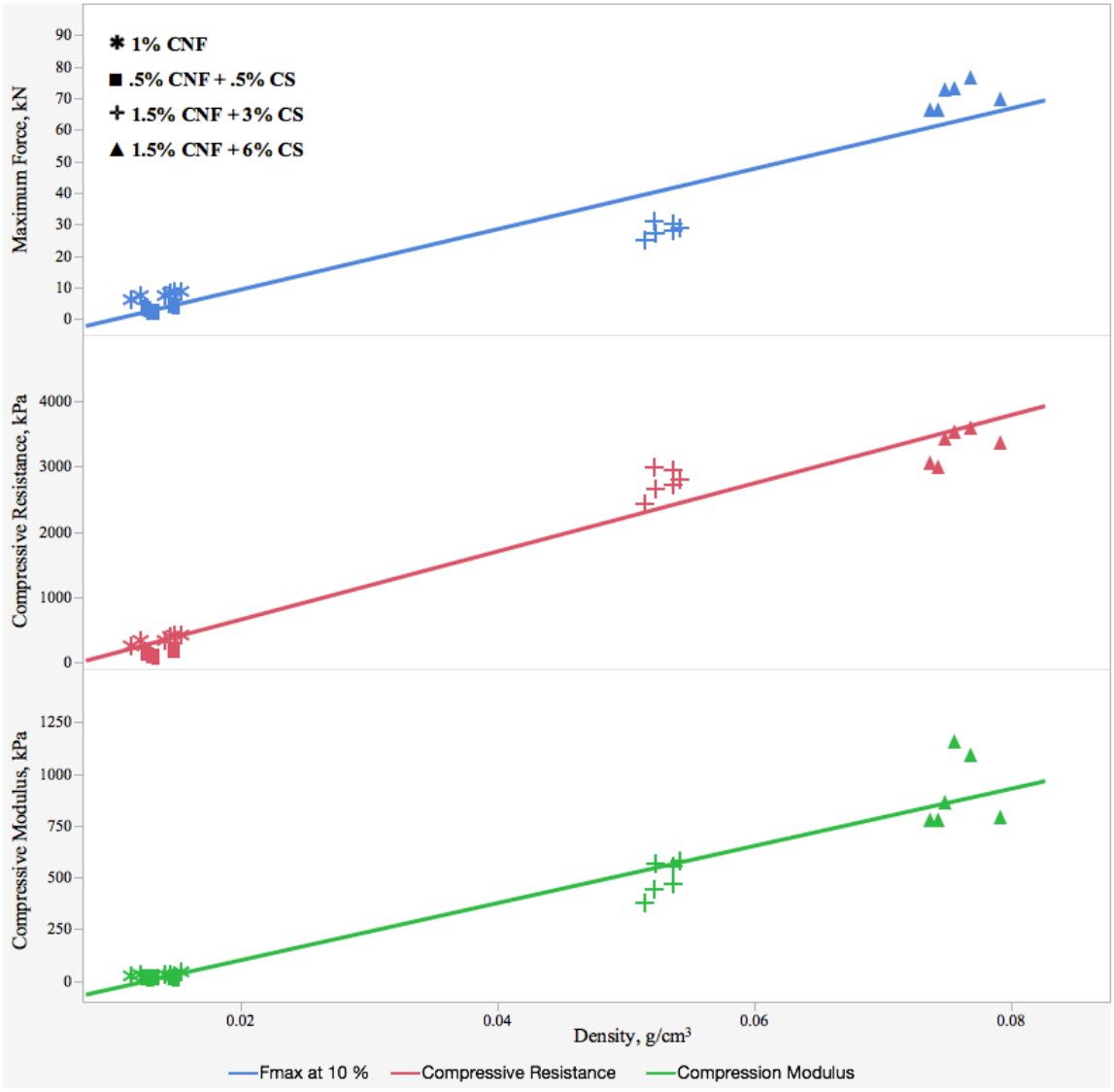

Figure 2.7: Maximum force applied when the foams were compressed up to 10% of original thickness.

Table 2.4: Compression properties of foams and comparisons with other studies.

Sample	Density (g/cm3)	Compressive Modulus (kPa)	Compressive Resistance (kPa)	Fmax at 10% (kg)
0.5% CNF + 0.5% Starch	0.014 (7.0) C	15.0 (13) C	144 (31) C	326.8 (30) D
1% CNF	0.014 (11) C	30.0 (23) C	359 (17) C	792.8 (14) C
1.5% CNF + 3% Starch	0.053 (2.1) B	496 (16) B	2753 (7.4) B	2897.3 (7.0) B
1.5% CNF + 6% Starch	0.076 (2.7) A	907 (19) A	3330 (7.5) A	7195.7 (6.1) A
7.5% Starch	N/A	N/A	N/A	N/A
Carbon foam (Wang et al., 2006)	0.73	-	6100	-
Gypsum board (Gypsum Association, 2010)	-	-	2750	-
CNF aerogel (Sehaqui and Berglund, 2011)	0.014	34.9	3.20	-
CNF aerogel (Sehaqui and Berglund, 2011)	0.029	199	24.4	-
CNF aerogel (Sehaqui and Berglund, 2011)	0.050	1030	69	-
CNF aerogel (Sehaqui and Berglund, 2011)	0.105	2800	238	-
CNF foam (Ali and Gibson, 2013)	0.016	62	-	-
CNF foam (Ali and Gibson, 2013)	0.027	249	-	-
CNF foam (Ali and Gibson, 2013)	0.063	1760	-	-

Note: Parentheses indicate the coefficient of variation (COV, %). A, B, C and D letters indicates the significant differences between the treatments.

The comparison of foam compression properties (Table 2.4) showed that the compression results for the foams produced in this study appear promising for applications such as insulation and packaging. (Sehaqui and Berglund 2011) reported that mechanical properties of CNF aerogel were positively correlated with density. The reinforced starch foams, which were produced in this study, have similar, comparable compression

properties with pure CNF foams, aerogels and some other insulation foams. Ali and Gibson (Ali and Gibson 2013) found that, the 2% solids CNF foams have 1760 kPa compression modulus with 0.063 g/cm3 density, whereas foams produced in this study (1.5% CNF + 6% S) have 907 kPa compression modulus with 0.076 g/cm3 density. Including 6% starch, and less CNF content in the foam structure produced lower mechanical properties.

Thermal conductivity and resistivity results (Table 2.5) indicated no statistically significant differences among the foam combinations, which have 4.5% or higher solids content in its structure. The pure CNF with 1% solids content showed higher thermal conductivity when compared to the other combinations where the lower thermal conductivity means better insulation.

The comparison of thermal insulation properties (Table 2.5) showed that the thermal conductivity and thermal resistivity results for the foams produced in this study appear promising like the compression properties. Foams produced in this study have 3 to 4 times better thermal resistivity properties when compared to gypsum board that has 0.83°F.h.ft2/BTU R-value (thermal resistivity) for 25.4 mm thickness (Gypsum Association 2010) and the foams have similar thermal conductivity with nanoporous silica aerogel impregnated highly porous zirconia ceramics have thermal conductivity from 0.041 W/m-K to 0.098 W/m-K (Hong et al. 2013). Mahlia et al. showed that thermal conductivities of some insulation materials as follows: fiberglass-urethane 0.021 W/m-K, fiberglass-rigid 0.33 W/m-K, urethane-rigid 0.024 W/m-K, perlite 0.054 W/m-K, extruded polystyrene 0.029 W/m-K and the urethane (roof deck) 0.021 W/m-K (Mahlia et al. 2007).

Table 2.5: Thermal conductivity and thermal resistivity properties of foams.

Sample	Density (g/cm3)	Thermal Conductivity (W/m-K)	R value (°F.h.ft2/BTU)
0.5% CNF+ 0.5%Starch	0.013 (5.1) D	0.048 (6.2) B	3.03 (11) B
1% CNF	0.014 (9.2) D	0.054 (7.4) C	2.87 (13) B
1.5% CNF+ 3%Starch	0.053 (2.1) C	0.047 (4.2) AB	3.60 (4.4) A
1.5% CNF+ 6%Starch	0.082 (5.9) B	0.042 (2.4) A	4.02 (1.5) A
7.5% Starch	0.098 (3.6) A	0.041 (4.8) A	4.14 (4.3) A
Gypsum Board (Gypsum Association, 2010)	-	-	0.83
Silica Aerogels (Hong et al., 2013)	-	0.041-0.098	-
Fiberglass-urethane (Mahlia et al., 2007)	-	0.021	-
Fiberglass-rigid (Mahlia et al. , 2007)	-	0.330	-
Urethane-rigid (Mahlia et al., 2007)	-	0.024	-
Perlite (Mahlia et al., 2007)	-	0.054	-
Extruded polystyrene (Mahlia et al., 2007)	-	0.029	-
Urethane (roof-deck) (Mahlia et al., 2007)	-	0.024	-
Granular Starch (Hsu and Heldman, 2004)	-	0.490	-
Gelayinized Starch (Hsu and Heldman, 2004)	-	0.470	-
Freeze-dried corn starch (Delilah et al., 1995)	-	0.040	-

Note: Parentheses indicate the coefficient of variation (COV, %). A, B and C letters indicates the significant differences between the treatments.

Hsu and Heldman showed that granular starch has 0.49 W/m-K thermal conductivity and gelatinized starch have 0.47 W/m-K thermal conductivity (Hsu and Heldman 2004), which have 9-10 times higher conductivity when compared the CNF reinforced starch foams produced in this study. Glenn and Irving showed that corn freeze-dried starch has a 0.040 W/m-K thermal conductivity (Delilah et al. 1995), which is similar to the values of experimental specimens due to similar production method and cellular structure of materials.

As a result of thermal analyses (Table 2.6), it was found 1% CNF foams have a higher thermal degradation point of (onset temperature; temperature at 10% weight loss) 277 °C when compared to the other combinations tested. (Oksman et al. 2007) indicated that the onset temperature of cellulose nanoparticles is between 200-300 (°C). The addition of starch consistently decreased onset temperature with reduction from 277 to 260 ˚C and 277 to 255 ˚C as initial starch concentration increased to 3 % and 6%. Switching the 0.5% CNF to 0.5% starch or adding more starch to the foam decreased the onset temperature.

Table 2.6: TGA and DTGA results for foams.

Sample	T, Weight loss 10%, °C	T, Weight loss 50%, °C	DTGA temp. °C	Mass loss (%)	Residue (%)
.5% CNF+ .5%Starch	276 (0.4) AB	320 (0.1) B	303 D	33.2 (5.2) D	14.4 (19) A
1% CNF	277 (2.2) A	335 (0.1) A	339 A	55.3 (1.2) A	15.3 (8.6) A
1.5% CNF+ 3%Starch	260 (1.4) ABC	308 (0.4) C	304 C	45.5 (1.6) B	8.70 (18) C
1.5% CNF+ 6%Starch	255 (4.7) C	318 (0.4) B	310 B	40.9 (3.4) C	11.6 (14) B
7.5% Starch	259 (0.7) BC	300 (0.1) D	295 E	43.3 (1.3) BC	14.9 (3.3) A

Note: Parentheses indicate the coefficient of variation (COV, %). A, B and C letters indicates the significant differences between the treatments.

The DTGA (derivative TGA) temperature (decomposition temperature) of cellulose was found between 315 °C – 400 °C by (Yang et al. 2007) and it was indicated in another study that cellulose has a sharp weight loss starting at 305 °C (Moran et al. 2010). In this study it was determined to be 338.6 °C for 1% CNF and when the starch was added to the structure. Two peaks were evident in the DTGA curves, one for starch and one for CNF (Figure 2.8b).

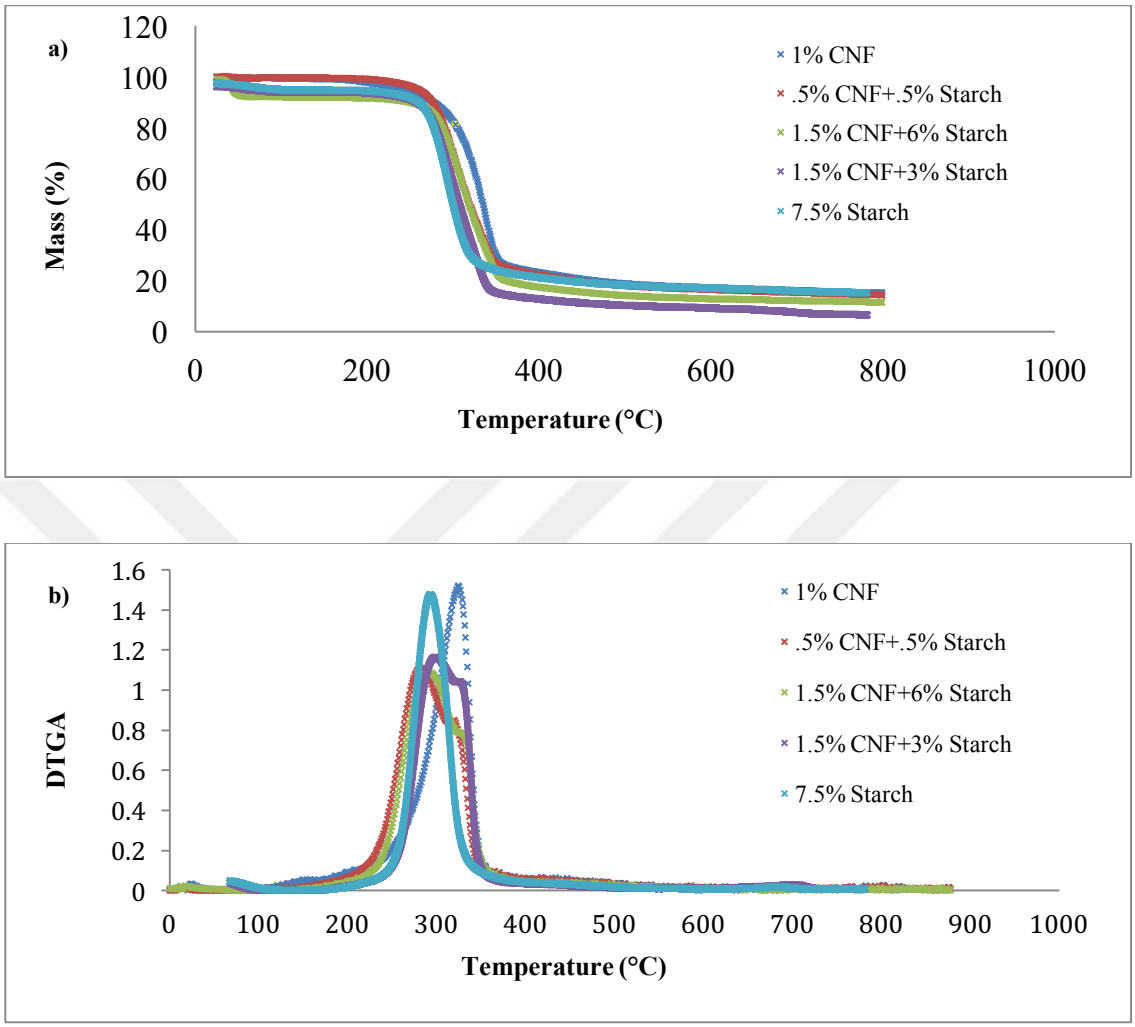

Figure 2.8: TGA and DTGA curves of foams.

(a) TGA curves. (b) DTGA curves.

DTGA temperatures were determined statistically different for CNF + starch combinations, whereas they showed similar results that changes between 303 °C to 310 °C.

2.10 Conclusions

Biodegradable and renewable foams produced in this study have highly porous microcellular structure includes foam walls of CNF material embedded within a starch

matrix. Because of starch`s low mechanical properties cellulose nanofibrils were used as a reinforce material which provided superior performance to starch foams. Increasing the CNF amount and increasing the density produced higher mechanical properties. The optimum properties were obtained from 6% Starch + 1.5% CNF combinations, which has promising mechanical and thermal properties when compared with previous studies. This study was an exploratory and that it has found promising results indicating excellent potential to use the CNF reinforced starch foams as a potential structural insulation material. Future work will include investigating the effect of CNF reinforcement for higher total loadings, creating a micromechanical model for different volume fractions and quantifying the hygroscopicity of the material and the effect of that on performance.

2.11 Acknowledgement

The author thanks The University of Maine Process Development Center for supplying cellulose nanofibrils in this study and thank Melanie Blumentritt's contribution of collecting the SEM images. This work partly supported by the USDA/NIFA under the Wood Utilization Research Program (Project 2010-34158-21182).

CHAPTER 3

CELLULOSE NANOFIBRIL (CNF) REINFORCED OPEN CELL FOAMS: APPLICATION OF CUBIC FOAM THEORY

3.1 Abstract

Cellulose nanofibril (CNF) reinforced open cell foams were produced using cellulose nanofibrils (up to 1.5% by weight), corn starch (up to 6% by weight), and water in conjunction with a freeze-drying process. As indicated in previous studies, starch foams are extremely friable and have low mechanical performance. The compressive performance of foams was significantly enhanced through incorporation of CNF. An inverse modeling scheme (back calculation) utilizing cubic array foam theory and the rule of mixtures for the CNF/starch foam wall material was used to predict the modulus of elasticity of the CNF component. Microscopic techniques (SEM and AFM) were used to measure the unit cell dimensions (beam/strut) as a function of CNF volume fraction. The prediction was that the CNF as a raw material has a 1.8 GPa compression modulus. Future studies will include the investigation of CNF compression modulus using AFM and nanoindentation techniques and will focus on the enhancements of mechanical properties.

3.2 Introduction

Cellular materials are made up from small compartments called cells. These cells have unique structures and interconnected through the cell walls, edges, faces or corners (Gibson and Ashby 1998). Cellular materials or cellular solids refer to a variety of porous structures including honeycombs, open-cell foams or closed cell foams. Raw materials for foam production can be polymers, metals, ceramics or organic materials. In

addition, foams can be found in nature with wood, cork, and bone as good examples (Michalska and Pecherski 2003). Foams are popular in applications which require materials with low thermal conductivities. Mechanical properties of the foams mostly depend on the materials that have been used to produce the foams (Gan et al. 2005) as well as density. In this study, we produced starch-based foams reinforced with cellulose nanofibrils. The main reason for using cellulose and starch is they both are biopolymers, compatible with each other and abundant in nature. Cellulose can be obtained from trees, a broad range of plants and even sea animals (Moon et al. 2010) while starch can be obtained from corn, potato, rice wheat etc. (Shogren et al. 1998).

The compression properties of organic composite foams were investigated using a hybrid model consisting of cubic array theory for the cellular structure with the rule of mixtures used to describe the mechanical properties of the CNF/starch foam wall material.

3.3 Materials and Methods

Five different organic composite foam combinations were produced with a variety of CNF/Starch/Water combinations (Table 3.1). Materials were corn starch and cellulose nanofibrils produced at the University of Maine pilot plant. Details on the manufacturing process can be found in Yildirim et al. 2014.

Table 3.1: Weight percent composition of freeze drying foam mixtures.

Foam Combinations	Solids Content
0.5% CNF+ 0.5%Starch	1%
1% CNF	1%
1.5% CNF+ 3%Starch	4.5%
1.5% CNF+ 6%Starch	7.5%
7.5% Starch	7.5 %

Density was measured for each material combination according to ASTM C303-10. Porosity measurements (calculations) were performed using porosimetry method followed by calculation provided earlier in Chapter 2 in equation 2.1 (Gibson et al. 1982).

Morphological properties and measurements of the cellular dimensions were conducted using scanning electron microscopy (Zeiss Nvision 40 FIB-SEM). Compression tests were conducted according to ASTM C165-07. Specimen displacements were obtained from the cross-head displacement. All physical and mechanical tests were conducted under the laboratory conditions of 25±2 °C temperature and 50% relative humidity.

3.4 Results and Discussion

3.4.1 Experimental Results

Produced foams were tested and investigated in our previous study (Yildirim et al. 2014). Foams produced in this study exhibited highly porous structures (93.5 % - 99.1 %) and low densities (0.013 g/cm3- 0.098 g/cm3). Morphological investigations showed that foams have mostly open cell structures (Figure 3.1a) and the cell wall structure is a plate of CNF material embedded within a starch matrix (Figure 3.1b,c). The fibril diameters typically ranged between 20 and 200 nm (Figure 3.1c).

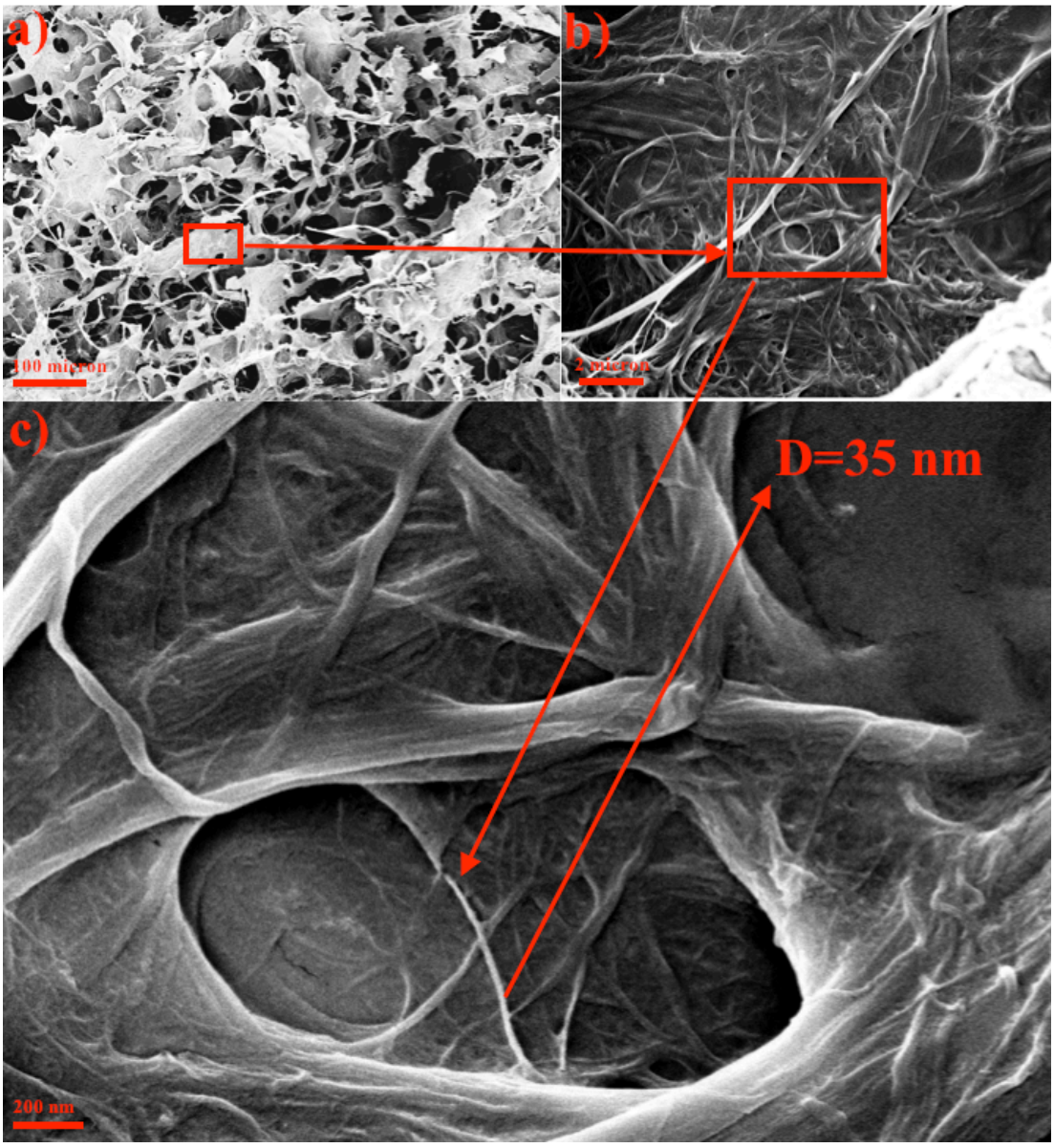

Figure 3.1: Representative SEM images of foams (1.5% CNF + 6% S).

(a) Cellular structure. (b) Distribution of nanofibrils in 2 micron scale bar. (c) Fibril diameter measurements.

A typical stress-strain curve for the compression tests is given in Figure 3.2. The compressive modulus (E) was obtained from the linear portion of the stress-strain curve by creating linear trendline on charts.

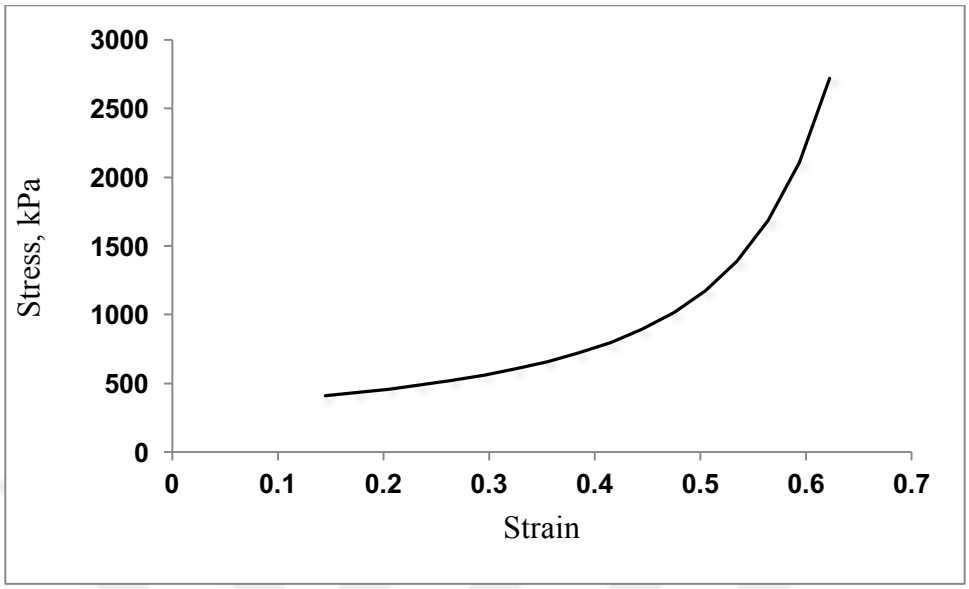

Figure 3.2: Typical stress-strain curve for compression tests of rigid foam boards.

Compressive properties are summarized in Table 3.2. Detailed information and comparison with other studies can be found in Yildirim et al. 2014.

Table 3.2: Compression properties of the foams.

Sample	Bulk Density (g/cm3)	Compressive Modulus (kPa)	Compressive Strength (kPa)
0.5% CNF+ 0.5%Starch	0.014 (0.0010) C	15.0 (2.0) C	144 (44.0) C
1% CNF	0.014 (0.0016) C	30.0 (7.0) C	359 (63.0) C
1.5% CNF+ 3%Starch	0.053 (0.0011) B	496 (82) B	2753 (203) B
1.5% CNF+ 6%Starch	0.076 (0.0020) A	907 (171) A	3330 (249) A
7.5% Starch	N/A	N/A	N/A

Note: Parentheses indicate the standard deviation. A, B, C and D letters indicates the significant differences between the treatments.

3.4.2 Microstructural Modeling Results

Cubic array foam theory for open cell foams was used (Gibson and Ashby, 1998). It was assumed that the produced foams were isotropic and that the cell wall material was linear-elastic. Relative density is defined as the ratio of bulk density (δ_{bulk}) to cell wall

density ($\delta_{material}$) (Eq. 3.2). For open cell foams, this relative density can be predicted from the idealized structure dimensions (Eq. 3.2.1).

$$\delta_{relative} = \left(\frac{\delta_{bulk}}{\delta_{material}}\right) \quad \text{Eq. 3.2}$$

For open cell foams;

$$\delta_{relative} = C_2 \left(\frac{t}{l}\right)^2 \quad \text{Eq. 3.2.1}$$

where;

t= beam thickness (7 microns, Table 3.3)

l=beam length or beam width (19 microns, Table 3.3)

C_2= 3/8, numerical constant (Gibson and Ashby 1998)

Usually, the given equations are enough for calculations however, if the relative density is large detailed simple expressions overestimate the final result. In this case, there are different calculations and suggested correction factors (D1, D2, D3, D4) for foam structure determination (open cell foam or closed cell foam). These correction factors can be significant when the relative density, which provides information about the cell wall thickness and the pore spaces, is especially equal or larger than 0.2 (Gibson and Ashby 1998). Since relative density of the experimental foams was around 0.05 - none of these corrections were necessary. The application of this approach is provided for foam combination 4 (1.5% CNF+ 6% Starch). The measured bulk density (δ_{bulk}) was 0.076 g/cm^3 and the material density ($\delta_{material}$) was assumed to be 1.5 g/cm^3.

The unit cell (cubic cell) column and beam dimensions (thickness and length) for a foam produced from 1.5% weight CNF and 6% weight starch were measured using scanning

electron microscopy. A minimum of 15 measurements were conducted for each dimension and the average values are reported (Table 3.3).

Table 3.3: Material properties of experimental CNF/starch foam.

	Material Properties	**1.5% CNF+ 6%Starch**
Unit cell dimensions	t, thickness (μm)	7
	L, length (μm)	19
Physical properties	$\delta_{material}$, material density (g/cm^3)	1.5
	δ_{bulk} , foam bulk density (g/cm^3)	0.076
	Relative density	0.051
	Φ, porosity (%)	94.95
Mechanical properties	E, compression modulus (kPa)	907

In open cell foams like the ones produced in this study, cell walls bend under compression forces (Gibson and Ashby 1998).

The cubic array formula for foam modulus (Equation 3.3) was rearranged and the required beam/column modulus was predicted based on experimentally determined foam modulus.

$$E_{foam} = E_{material}\ x\ C_1\ x\ \left(\frac{\delta_{bulk}}{\delta_{material}}\right)^2 \quad \text{Eq. 3.3}$$

where;

$E_{material}$= Modulus of the beam and columns

E_{foam}= Foam modulus

C_1= 1, Numerical constant (Gibson and Ashby 1998)

The foam wall material is a composite material composed of starch (matrix) and CNF (fibers). The properties of the cell wall material was assumed to be described by the rule of mixtures (Eq. 3.4 & Eq. 3.4.1) (Reuss 1929).

$$E_{material} = V_f\ x\ E_f + \left(1 - V_f\right)\ x\ E_m \quad \text{Eq. 3.4}$$

$$V_f = \left(\frac{\text{Volume of Fibers}}{\text{Volume of Fibers} + \text{Volume of Matrix}}\right) \quad \text{Eq. 3.4.1}$$

where;

$E_{material}$= Composite modulus (foam cell wall material)

E_f= Fiber modulus (modulus of elasticity of CNF)

E_m=Matrix modulus (modulus of elasticity of starch, 2.9 MPa (Glenn and Irving 1995)

V_f=Fiber volume fraction (0.2)

The material (composite cell wall) modulus predicted by Equation 3 was assumed to be equal to the $E_{material}$ of equation 4. This resulted in an estimate of 1.8 GPa for the fiber (CNF) modulus. In the calculations given above (Eq. 3.4 and Eq. 3.4.1) rule of mixtures assumes all fibers are perfectly aligned and that the fibers are continuous, the aspect ratio of the CNF exceeds 100 and therefore the assumption of continuous fibers is reasonable.

Comparison of this indirect estimate of fiber modulus with direct experimental measures is relevant. Cheng and Wang studied the elastic modulus of a single cellulose fibril using atomic force microscopy. They applied three point bending test and determined that the elastic modulus of single cellulose fiber with 170 nm diameter was 93 GPa (Cheng and Wang 2008). (Eichorn and Young 2001) investigated the Young's modulus of microcrystalline cellulose using Raman spectroscopy and estimated the modulus to be 25±4 GPa. A recent study was done by Moon et. al on the elastic properties of crystalline cellulose Iβ showed that Young's modulus varies in 3 directions, with estimates of 19 GPa at weakest axis and 206 GPa in the strongest axis (Moon et al. 2013). (Lahiji et al. 2010) investigated the single cellulose nanocrystal properties using atomic force microscopy and determined that the transverse modulus of single cellulose nanocrystals

varies between 18 and 50 GPa. Another study on cellulose nanocrystals by (Wagner et al. 2011) and showed that the transverse elastic modulus of CNC is 8.1 GPa with a 95% confidence interval of 2.7-20 GPa. The predicted modulus of cellulose nano particles and nanofibrils varies significantly in each study. Many of the studies explored crystalline cellulose. However, the CNF in this study has amorphous structures in the fibrils. This can be expected to decrease the mechanical properties significantly. Another reason for the lower estimate may be attributable to the irregularities and imperfections in the foam structure (Figure 3.3). Imperfections due to shape differences, gaps and cracks (Fig. 3.3a) can be caused because of drying process. In addition, there are some heterogeneities (poor fibril dispersion) and there was variation in the embedment of CNF in the foam wall starch matrix (Fig. 3.3b). Any foam beam/column element which were primarily starch would be expected to fail at lower stresses.

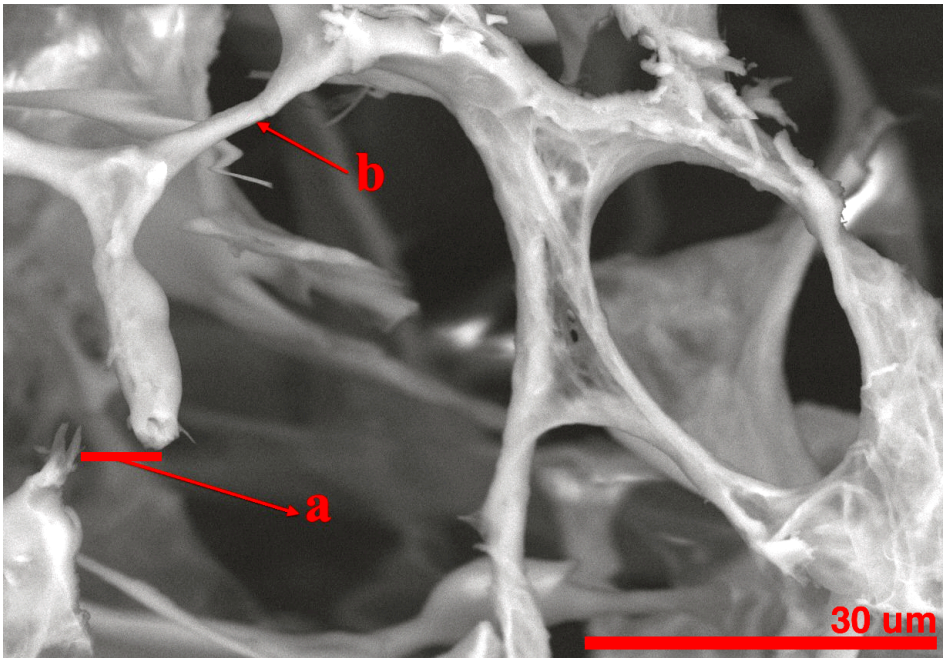

Figure 3.3: Structure imperfections and irregularities.

3.5 Discussions and Conclusions

In this paper, the compressive modulus of cellulose nanofibrils were predicted using bulk property measurements and an inverse hybrid theoretical model composed of foam theory and the rule of mixtures. As expected, density had a significant effect on the mechanical properties of the foams with lower density correlated with lower mechanical performance. The mechanical performance of the foam can be enhanced by modifying the foam structure during production process or can be increased by the addition of cellulose nanofibrils. The CNF modulus was predicted to be 1.8 GPa using the inverse hybrid modeling approach. Literature values from direct experiments on crystalline cellulose are significantly higher. The idealized open cell foam model did not account for a variety of factors (e.g. structural irregularities, imperfections, different fibril diameters and heterogeneous fibril dispersion).

CHAPTER 4

NANOMECHANICAL PROPERTIES OF CELLULOSE NANOFIBRILS (CNF)

4.1 Abstract

Cellulose is an abundant green polymer, which can be obtained in a variety of nanoscale structures broadly grouped as nano/microfibrils (CNF/MFC), bacterial celluloses (BC) or nano/microcrystals (CNC/CMC). There is increasing interest in nanocelluloses by the research and industrial communities attributable to increasing available materials (facilities than can produce ton per day), impressive strength properties, low density, renewability and biodegradability. However, one problem is the lack of knowledge on the nanomechanical properties of cellulose nanofibrils, which creates barriers for the scientists and producers to optimize and predict behavior of the final product.

In this research, the behavior of thin films ($t \leq 100$ μm) of cellulose nanofibrils', located on aluminum pin stubs, under nano compression loads were investigated using an Asylum Research MFP-3D Atomic Force Microscope equipped with a nanoindenter. Unloading curves were analyzed using Oliver-Pharr. As a result of 58 successful nanoindents, the average modulus value was estimated as 16.6 GPa with the reduced modulus value of 18.2 GPa. The CNF Modulus values varied between 12.4 GPa – 22.8 GPa with 16.9% coefficient of variation (COV) while the reduced modulus ranged from 13.7 GPa to 24.9 GPa with a 16.2 % COV.

This research provides practical knowledge for producers of nanocellulose, researchers and applications developers who focus on nanocellulose reinforced composite materials.

4.2 Introduction

Cellulose is a biopolymer, which can be isolated from nature (woods, plants, bacteria and even animals) (Moon et al. 2010 and Eichorn et al. 2010). CNFs have received much attention because of their low density, nonabrasive, combustible, nontoxic and biodegradable properties (Kalia et al. 2011), which makes them suitable for the reinforcement material in composite structures (Cheng et al. 2009).

Previous studies have evaluated the nanomechanical properties of nanocellulose to understand its role in the composite structures. The elastic modulus of regenerated cellulose fibers (Lyocell) was determined as between 12 GPa and 17 GPa while that of viscose cellulose fibers to vary between 7 GPa and 13 GPa (Gindl et al. 2006).

These impressive mechanical properties and the increased availability of large volumes of material (multiple facilities are in place in North America and Europe with production capacities up to 2000 lb per day) have made these organic polymers more attractive for the industry and the researchers. However, the limited knowledge on the nanomechanical properties (Josefsson et al. 2014) of cellulose nanofibrils creates an opportunity for research to provide information, which will be of value to the research community and industry.

In this study, the nanomechanical properties of the cellulose nanofibrils (CNFs) were determined using a nanoindentation technique and an MFP-3D Atomic Force Microscope (AFM) equipped with a Nanoindenter (Asylum Research).

4.3 Materials and Methods

4.3.1 Sample Preparation

Softwood cellulose nanofibril suspensions were produced at the University of Maine Process Development Center. The solids content (3.4% by wt.) of the CNF suspension were determined (Denver IR 35 Moisture Analyzer). The suspension was poured into 1.5 mL polypropylene graduated microcentrifuge tubes and ultrasonicated for 1 hour (VWR 550 HT Ultrasonic Cleaner). The ultrasonicated suspension was centrifuged (Eppendorf Minispin Plus) at 14,500 rpm for 10 minutes. The transparent (liquid) portion, diluted portion was placed on aluminum pin stubs, dried at 30 °C for 1 hour, and then located in the heat controlled AFM chamber (24±1 °C) for 24 hours.

4.3.2 Analysis Tool and Nanoindentation Technique

The atomic force microscope is a tool invented in 1986 by Bining, Quate and Gerber (Bining and Quate 1986), which allows high-resolution 3D imaging of the material surfaces (Butt et al. 2005). It also enables the determination of nanomechanical properties of the materials providing force-distance curves. In this research, an Asylum Research MFP-3D Atomic force microscope equipped with a Nanoindenter was used for 3D imaging and nanomechanical measurements. All samples were imaged using tapping mode (non-contact or AC mode) with an Asylum Research AC240TS-10 cantilever tip with a 9±2 nm radius. The spring constant (k) was =2 N/m (0.5-4.4). The first scanning area was chosen 40 micron X 40 micron to understand and evaluate the fibril distribution, than zoomed to the 5 micron X 5 micron area.

Nanoindentation is a technique, which allows determination of the nanomechanical properties of materials. As with any experimental method – it is vital that the procedure used is repeatable and that the instrument is calibrated (Briscoe et al. 1988).

In this study, the indenter tip was imaged, particles and dusts on the tip surface cleaned and the area was calculated according to the tips' geometrical shape. The tip was then installed in the Asylum Research MFP-3D Nanoindenter Head located in a temperature-controlled chamber for 24 hours. After the thermal equilibration period, the device was calibrated. Additional detail on the experimental procedures and analytical assumptions are below.

4.3.3 Indented Area Calculation & Assumptions

The tip used in the integrated nanoindenter was of the Berkovich type. The area of the Berkovich tip was calculated according to its geometrical shape (Equation 4.1).

$$A=24*hc^2 \qquad \text{Eq. 4.1}$$

where;

A = Area (μm2)

hc = Contact depth (nm)

The contact area calculation (Eq. 1) assumes that: 1) The Berkovich tip is geometrically perfect, and 2) the area created on the sample surface is identical to the Berkovich tip area. Because of the significant impact of these assumptions, precautions were taken to ensure a clean tip.

4.3.4 Berkovich Tip Cleaning

A cotton swab was made fluffy by gently pulling the cotton part prior to soaking in ethyl alcohol. Tip cleaning was performed by wiping in one direction, from the threaded end to the tip of the Berkovich probe. The images of the Berkovich tip before cleaning (a) and after cleaning (b) is given in figure 4.1.

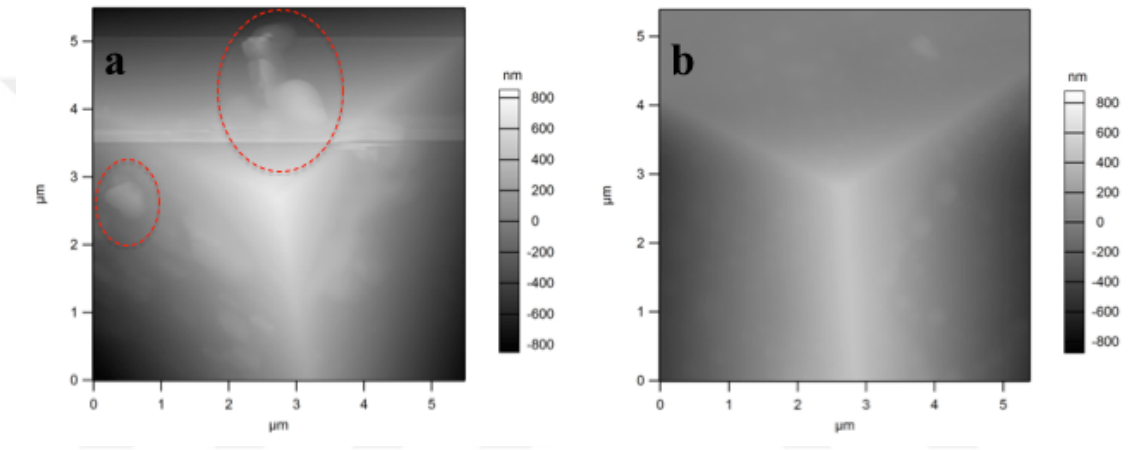

Figure 4.1: Berkovich tip.

a) Before cleaning the dust particles (red circled). b) After cleaning.

4.3.5 Calibration & Evaluation of Nanoindents

The nanoindenter was calibrated using sapphire ball (indenter) and sapphire samples. A three (3)-segment procedure which was comprised of loading, hold time and unloading were applied to create the nanoindents on the sample surface. Load-displacement (force-indentation) curves were evaluated by means of the Oliver-Pharr method (Oliver and Pharr 1992).

The Oliver-Pharr method uses the recorded load-displacement curves by relating the geometrical measurements. For a given tip indentation (displacement) – the contact area is calculated (Eq. 4.1). Then, stiffness (S) was calculated from the unloading portion of

the curve, which is needed to then calculate the reduced modulus. The reduced elastic modulus was determined (equation 4.2), which provides direct information about the materials' nanomechanical properties by recording the instantaneous response of the material to the applied force.

$$E_R = \frac{1}{2}\sqrt{\pi}\frac{S}{\sqrt{A}} \quad \text{Eq. 4.2}$$

where;

E_R = Reduced elastic modulus (GPa)

S = Stiffness (nN/nm)

Finally, the elastic modulus (E) of the material were calculated using the material and tip properties as given in equation 4.3.

$$\frac{1}{E_R} = \frac{(1-\nu^2)}{E} + \frac{(1-\nu_i^2)}{E_i} \quad \text{Eq. 4.3.}$$

where;

E: Elastic modulus of the sample (GPa)

ν: Poisson's ratio for the sample, 0.3 (Nakamura et al. 2004)

E_i: Elastic modulus of the tip (GPa), 865 (provided by the manufacturer)

ν_i: Poisson's ratio for the tip, 0.2 (provided by the manufacturer)

4.4 Results and Discussion

4.4.1 Morphological Properties

Representative CNF samples were imaged as thin films (t≤100 μm) using AFM in different scan areas from 1 μm^2 to 100 μm^2 to investigate the distribution of fibril diameters. The representative AFM images are given in Figure 4.2.

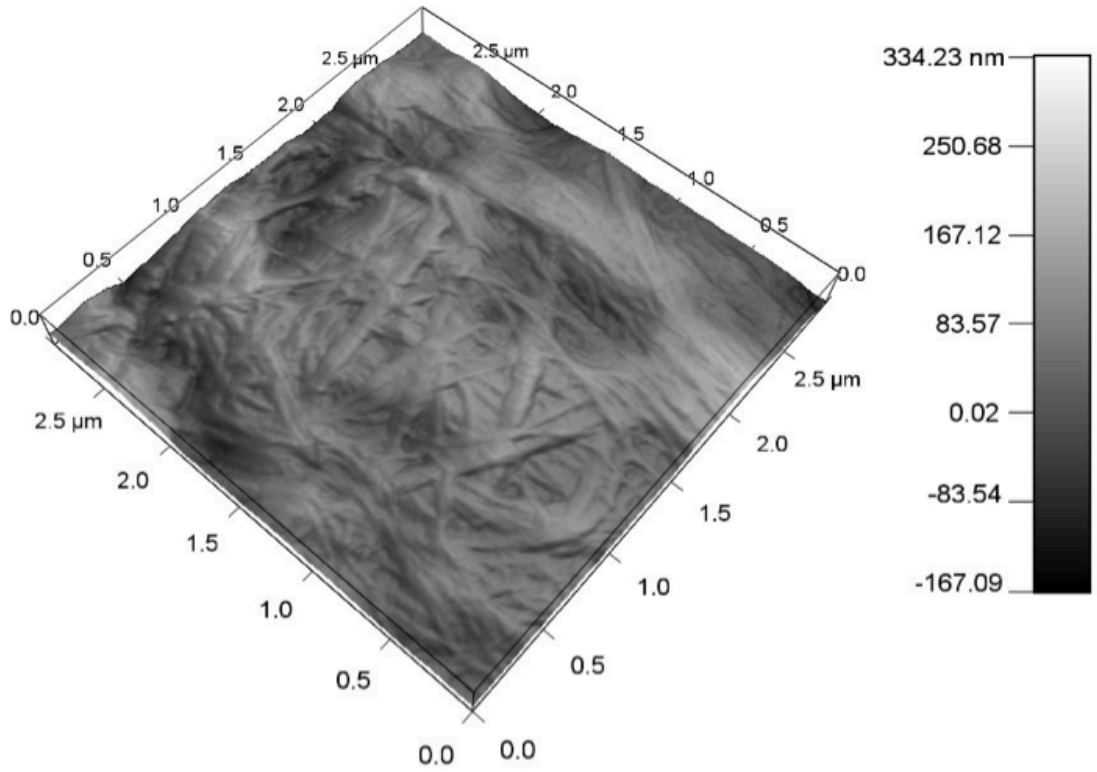

Figure 4.2: Representative 3D image of CNFs on aluminum pin stub.

As it is shown in Figure 4.2, Cellulose fibrils were obtained in micro scale and these microfibrils branched to the nanofibrils horizontally on the aluminum pin stubs. The significant characteristic of mechanically produced cellulose nanofibrils is the variety in the fibril diameters. The separated fibrils in this study varied between 20 nm to several hundred nanometers.

4.4.2 Nanomechanical Properties

More than 100 nanoindents were randomly created on CNF samples perpendicular to the fiber length direction. Each load displacement curve was evaluated and categorized as valid or not. Specifically, curves that exhibited a stiffening effect (Figure 4.3a) were discarded. Such behavior is speculated to occur attributable to complex geometric

assembly of nanofibrils on the stub tip. Specifically, it is postulated that 1) the tip may slide laterally off the rounded surface, and/or 2) the contacted nanofibril may have deformed and interacted with adjacent nanofibrils. Only indents with a classical response (Figure 4.3b) were used for analysis. A total of 58 of the 100 curves were judged valid.

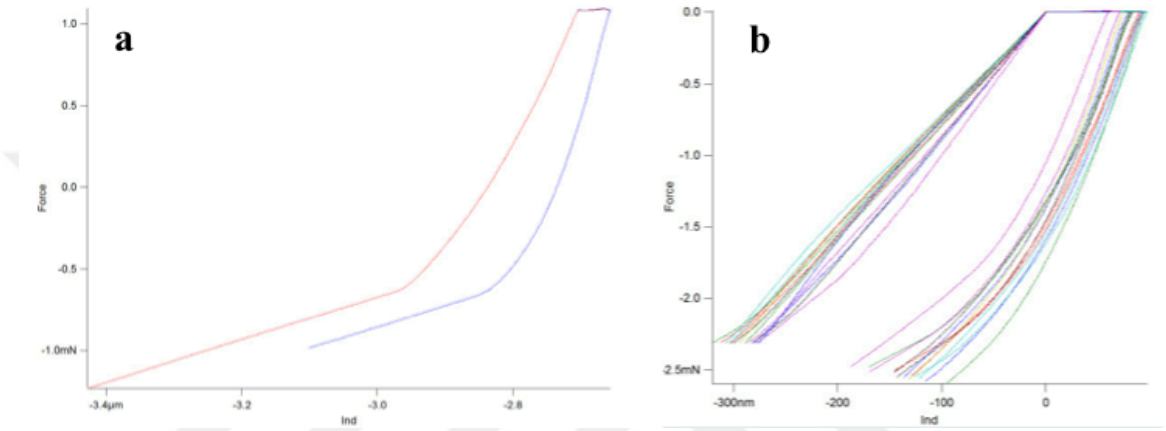

Figure 4.3: Representative nanoindentation curves.

a) Rejected nanoindents. b) Successful nanoindents.

Calculated CNF modulus, CNF reduced modulus, and the average contact depth values are summarized in Table 4.1. Also, a detailed comparison of the CNF modulus values from recently performed similar studies is given in Table 4.2.

Table 4.1: The nanomechanical properties of CNF.

Method	N, # of indents	CNF Modulus, GPa	CNF Reduced Modulus, Gpa	Hc, contact depth, nm
Oliver-Pharr	58	16.58 (16.9)	18.22 (16.2)	87.4 (16.3)

Note: Parentheses indicate the coefficient of variation (COV, %).

The average contact depth created on the CNF surfaces through nanoindentations was 87.4 nm with a 16.3 % coefficient of variation. The reduced modulus (E_R) was found

18.22 GPa with 16.2 % coefficient of variation. The estimated modulus (E) was 16.58 GPa with a 16.9% coefficient of variation.

Table 4.2: Modulus value comparison with other studies.

Material	Test instrument	Test Method	E (GPa)	Researcher
CNC	AFM	Compression	12.8	Pakzad et al. 2012
MCC	AFM - NI	Compression	3.5	Krishnamachari et al. 2012
CNC	Prediction	-	5.1	Wu et al. 2013
CNC	Theoretical	-	6.5-24.5	Wu et al. 2014
CNF	AFM - NI	Compression	15.8	Yildirim et al. 2015

The CNF modulus values obtained in this work have similar or higher modulus values than the previous studies. This is to be expected given the differing test methods, different raw materials, different moisture contents, different chamber temperature and nanomaterial production process. Further discussion is provided in Chapter 5.

In this study, it is shown that CNF modulus varies between 12.4 GPa – 22.8 GPa which is comparable with previous studies.

4.5 Conclusion

In this work, the nanomechanical properties of cellulose nanofibrils (CNFs), under compression forces perpendicular to its fiber direction, were investigated and reported. The mechanical production process produced significant heterogeneity in fibril diameters, which ended up with problems respectively unstable fibrils, tip sliding, and indentation failures through nanoindentation. These significant application problems were overcome by applying more than 100 nanoindents and using only the flawless, successful nanoindents for the evaluation. This research showed that Oliver-Pharr method is applicable for cellulose nanofibrils however; the Berkovich tip should be cleaned

carefully before the nanoindentations to prevent incorrect area calculations attributable to particles on the tip, which directly affects the results.

The nanomechanical properties of the CNFs were discovered in this research. Future work will include investigating the nanomechanical properties of the CNFs through different nanoindentation methods and approaches.

CHAPTER 5

THE APPLICATION OF NANOINDENTATION FOR DETERMINATION OF CELLULOSE NANOFIBRILS' (CNF) NANOMECHANICAL PROPERTIES

5.1 Abstract

Nanocellulose is one of the most impressive, eco-friendly organic polymers and is gaining strong interest in automobile, construction, insulation, packaging, and even aerospace industries. The expected global market for nanocellulose is $300 million by 2020 (BCC Research). These superb organic polymers can be isolated from nature (woods, plants, bacteria, and from sea animals) through chemical or mechanical treatments, as cellulose nanofibrils (CNF), cellulose nanocrystals (CNC) or bacterial celluloses (BC). Focused global research activities have resulted in decreasing costs. A nascent industry of producers has created a huge market interest in CNF. CNF can be utilized in composite structures as a reinforcing material or as a matrix attributable to its impressive mechanical, thermal and morphological properties. However, there is still lack of knowledge on the nanomechanical properties of cellulose nanofibrils, which create barriers for the scientist and producers to optimize and predict behavior of the final product. In this research, the behavior of CNF under nano compression loads were investigated through three different approaches, Oliver-Pharr (OP), fused silica calibration (FS), and tip imaging (TI) via nanoindentation in an Atomic Force Microscope. The average contact depth was 87.4 nm (n=58). The CNF modulus estimates for the three approaches were 16.6 GPa, for OP, 15.8 GPa for FS, and 10.9 GPa for TI. The CNF reduced moduli estimates were consistently higher and followed the same estimate rankings by analysis technique (18.2 GPa, 17.4 GPa, and 11.9 GPa). Variation in

CNF Modulus values (range and Coefficient of Variation (%)) were: 12 GPa to 23 GPa / 16.9% for OP, 12 GPa to 21 GPa / 13.2 % for FS, and 8 GPa to 15 GPa / 14.5 % COV for the TI approach. This unique study minimizes the uncertainties related to the nanomechanical properties of CNFs and provides increased knowledge and improvement on understanding the role of CNFs as a reinforcing or matrix material in composite structures and also improvement in making accurate theoretical calculations and predictions.

Keywords: Cellulose nanofibril (CNF), Atomic Force Microscope (AFM), Nanoindentation (NI), Nanomechanical Properties

5.2 Introduction

Nanocellulose, which can be obtained from wood, plants, bacterial cellulose and even sea animals (Moon et al 2010), is a renewable, eco-friendly nanomaterial with outstanding mechanical and thermal properties. These outstanding properties make nanocellulose a perfect candidate for reinforced materials used in composite structures. Nanocellulose can be prepared in different forms including cellulose nanofibrils (CNF), cellulose nanocrystals (CNC) or bacterial celluloses (BC). If the diameters of the fibrils or the particle size of crystals are at micron scales they are described as cellulose microfibrils (CMF), microfibrillated cellulose (MFC) or microcrystalline cellulose (MCC) (Siro and Plackett 2010). CNF makes up the largest volume of nanocellulose material produced, accounting for more than half of the nanocellulose market according to BCC (BCC Research LLC) Market research and projected to reach over $150 million by 2020.

In this study, the behavior of cellulose nanofibrils under nano compression forces were investigated through different approaches through nanoindentation technique using an Asylum Research MFP 3D Atomic Force Microscope (AFM) fit with a Nanoindenter (NI).

In recent years, there has been increasing interest in development of nanocomposites based on nanocellulosic materials (Siro and Plackett 2010). Recent regulations and requirements of environmental waste management policies push researchers to focus and create biomaterials produced using organic polymers like cellulose (Frone et al. 2011). The lack of knowledge on the nanomechanical properties (Josefsson et. al 2014) of the CNFs creates a barrier to predicting the mechanical behavior of composites composed of said material.

This research aimed to determine the nanomechanical properties of the CNFs produced through a mechanical process.

5.3 Materials and Methods

CNF used in this study was produced through a mechanical process at the Process Development Center (PDC) at the University of Maine. A double disk refiner was used to nanofibrillate a softwood bleached Kraft pulp. The produced materials typically have a diameters ranging between 20 and 100 nm and lengths on the order of several micrometers.

5.3.1 Sample Preparation

The samples for the calibration and the nanoindentation were produced as thin films through oven and air drying (Figure 5.1). CNF/water suspensions were obtained at 3.4 %

solids by weight with the solid content controlled using moisture content analyzer (IR35M – Denver Instrument Germany). The CNF suspensions were poured into the micro centge tubes (1.7 ML. capacity - TedPella) using disposable syringes (1 mL. – TedPella). The suspension was ultrasonicated for 1 hour (VWR - 550HT). The ultrasonication was followed by centrifuging for 10 minutes at 14,500 revolutions per minute (Eppendorf MiniSpin Plus). Samples obtained from the transparent fraction (i.e., the diluted part) of the suspension were dropped on aluminum pin stubs (ϕ12.7 mm x 8mm pin height) and dried for 2 hours (maximum) at 30 °C. The partially dried samples were placed into the temperature-controlled Atomic Force Microscope (AFM) chamber (25±1°C) for air drying for 24 hours before calibration and the actual tests.

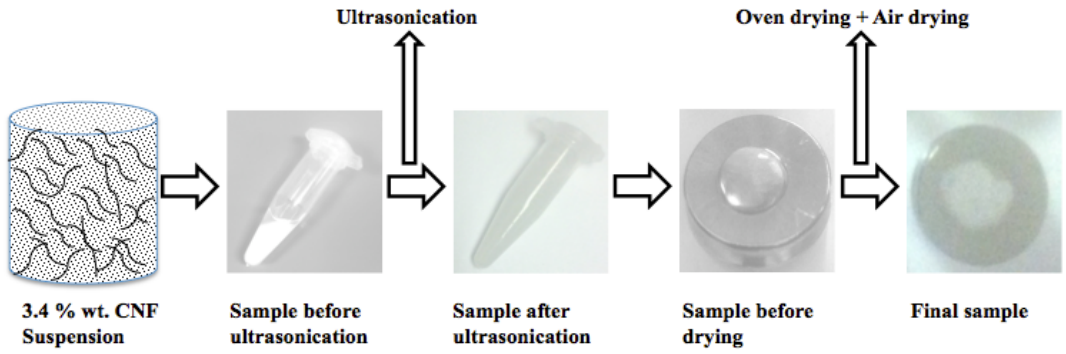

Figure 5.1: Sample preparation procedure.

The heterogeneity in dimensions of the CNFs produced presented experimental challenges. Therefore, large numbers of tests (n=58) and 3 different data analysis approaches were conducted. The experimental design of the study is given in Table 5.1.

Table 5.1: Experimental design of test samples.

Sample	Number of Pin Stubs	Calibration		CNF Tests	
		Approach	N, number of indents	Approach	N, number of indents
3.4 % CNF	10	Oliver Pharr (OP)	60	Oliver Pharr (OP)	58
		Tip Imaging (TI)		Tip Imaging (TI)	
		Fused Silica (FS)		Fused Silica (FS)	

5.3.2 Nanoindentation

The calibration was performed using a "sapphire sample – sapphire ball probe." The sapphire ball probe was moved up and down at least 20 μm further away from the sapphire sample surface and the potential virtual deflection were determined. Then, high force curve was performed on the flat sapphire sample and the optical lever sensitivity (DefI InvOLS) was determined, which provides conversion from voltage signal (DeflVolts) to displacement units (deflection). The spring constant provided from the manufacturer (k=2,416.26 N/m), was used for all calculations.

The force – indentation curves obtained from experimental tests were evaluated according to Oliver Pharr method (Oliver and Pharr 1992). However, the contact area (A) was calculated through three different approaches: Oliver Pharr (OP), tip imaging (TI) and fused silica (FS).

5.3.2.1 Oliver Pharr (OP)

Using the OP approach, the indented area was calculated according to geometrical area calculations of a perfect Berkovich tip area (Equation 4.1). It is further assumed that the indented area on the sample surface is identical with the tip area.

$$A = 24.5 \times h^2 \qquad \text{Eq. 5.1}$$

Where: h = depth of indentation

5.3.2.2 Tip Imaging (TI)

In the second approach, the Berkovich tip was imaged using AFM in non-contact mode (Figure 5.2). A third order polynomial function ($A=C0h_c^2+C1h_c+C2h_c^{1/2}$), was used to describe imaged tip area as a function of indentation depth (h_c). As in the case of the OP approach, the indented area of the sample surface was presumed identical to the tip area function.

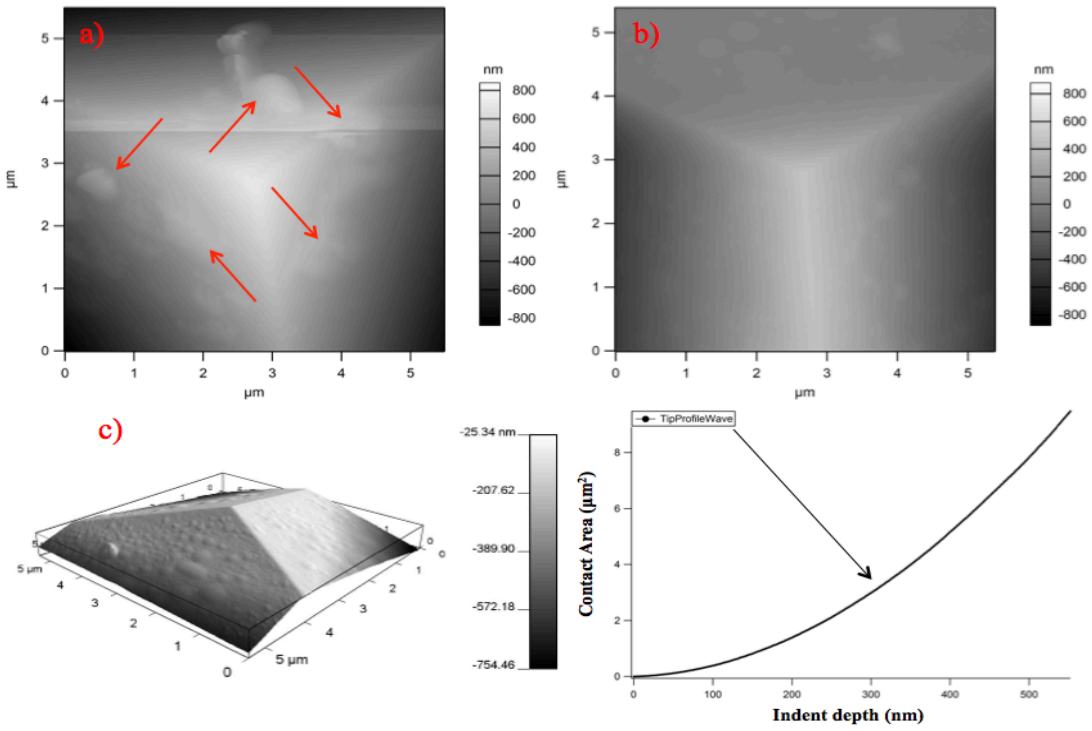

Figure 5.2: Representation of the Berkovich tip imaging and tip area function.

a) Imperfections on the tip. b) 2-D view of the Berkovich tip. c) 3-D view of the Berkovich tip. d) The area function according to actual Berkovich tip.

5.3.2.3 Fused Silica (FS)

In the last approach, FS samples were nanoindented using an Asylum Research Nanoindenter (MFP 3D Atomic Force Microscope) fitted with a diamond Berkovich tip (Micro Star Technologies) (Table 5.2).

Table 5.2: Nanoindentation tip dimensions and geometry.

Dimension	Nominal	Measured	Uncertainty	Units
Angle - a_1	65.30	65.27	±0.025	°
Angle – a_2	65.30	65.08	±0.025	°
Angle – a_3	65.30	65.42	±0.025	°
Angle - b_{12}	120.00	119.93	±0.025	°
Angle - a_{13}	240.00	239.82	±0.025	°
Radius - R	≤50	≤50	-	nm
Indentation Depth - h	2	2	-	µm

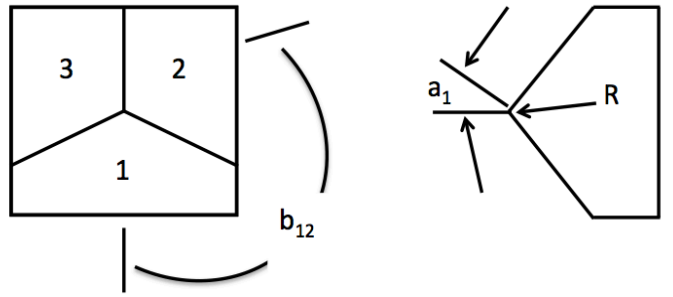

A total of 64 nanoindents (8x8 array over a 20 µm X 20 µm scan area) were conducted as shown in Figure 5.3.

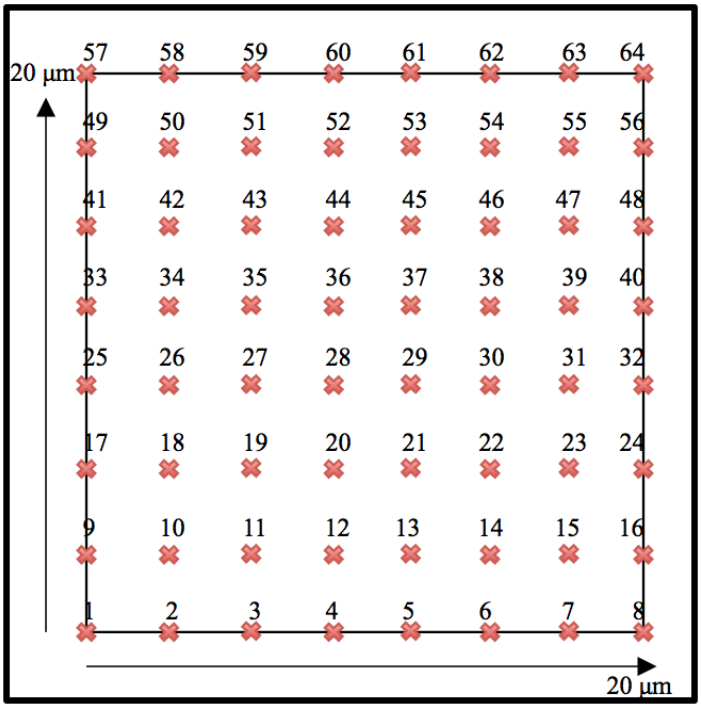

Figure 5.3: Representation of nanoindentaion application map.

For each indent (Figure 5.3), an IndentTriangleDwell function was used. Test samples were loaded at 125 µm/s with a dwell time of 2 seconds at the target load, following by unloading at the same speed rate, 125 µm/s as suggested by the manufacturer (Figure 5.4).

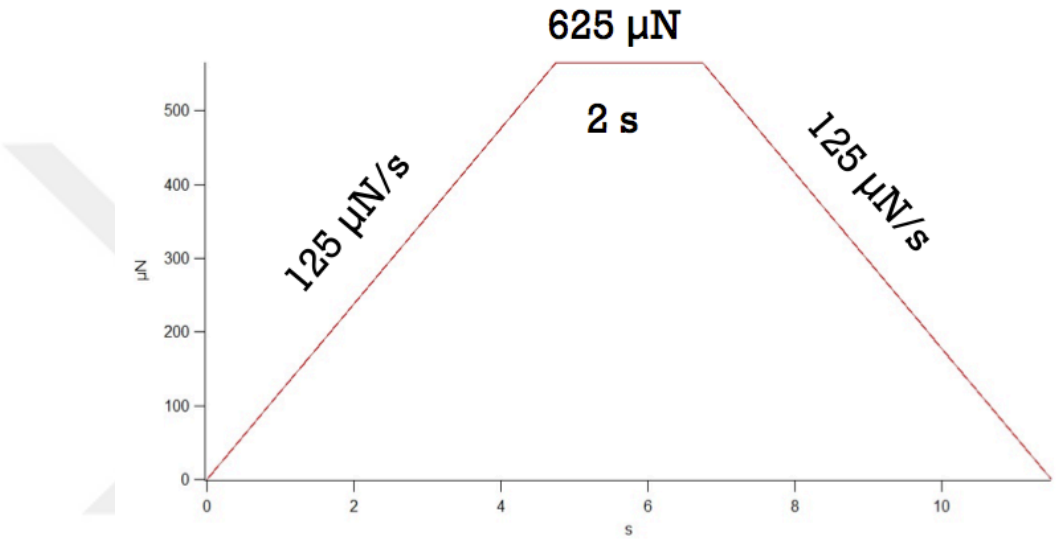

Figure 5.4: Sample loading and unloading procedure.

The actual modulus value of the tested fused silica quartz specimen (68 GPa-72 GPa) was provided by Asylum Research. The modulus values of fused silica quartz sample were calculated according to the Oliver Pharr approach. The difference between the calculated and actual modulus was determined and used to develop a correction function.

5.3.2.4 Nanoindentation on Nanocellulse

The stiffness value (S) of the 58 nanocellulose samples was determined using the slope of the unloading curve (Figure 5.5).

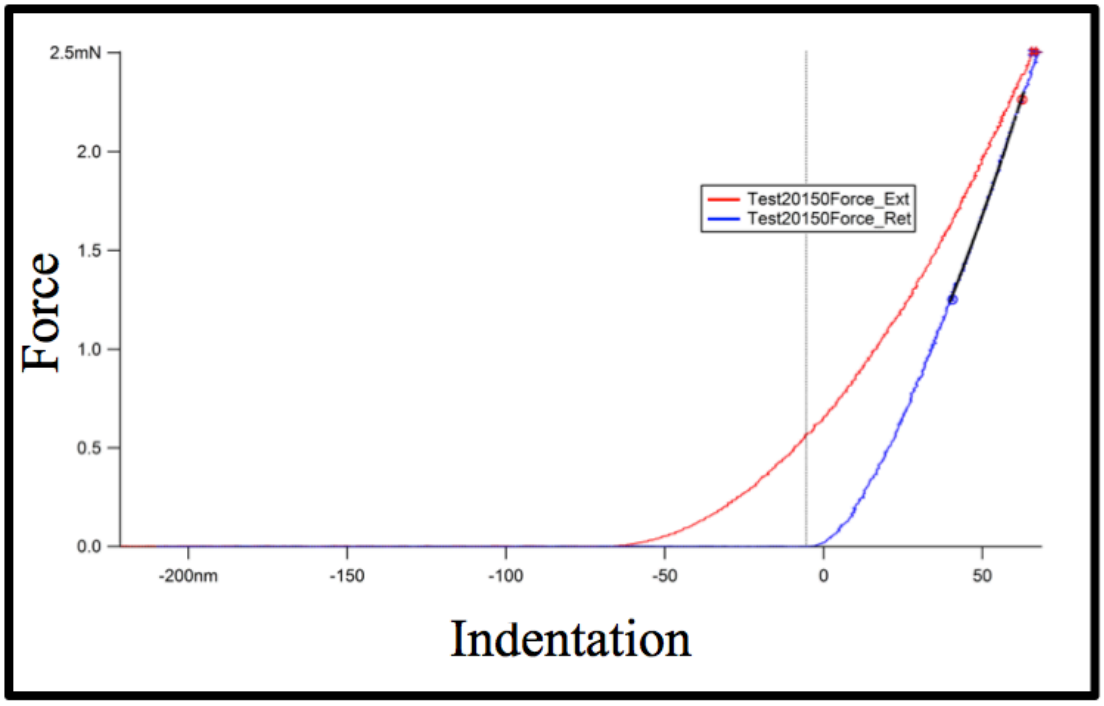

Figure 5.5: Representative loading and unloading curves.

The indented area (A) was calculated at 50 nm to couple hundred nm H_c range using the three different approaches previously described (OP, TI and FS). The reduced modulus (E_R) was then calculated (Equation 5.2).

$$E_R = \left(\frac{S\sqrt{\pi}}{2\sqrt{A}}\right) \qquad \text{Eq. 5.2}$$

Equation 5.3 was then used to calculate E_{CNF}.

$$E_{CNF} = \left(\frac{1-\nu_{CNF}{}^2}{\frac{1}{E_R}-\frac{1-\nu_{ind}{}^2}{E_{ind}}}\right) \qquad \text{Eq. 5.3}$$

The E value of the diamond Berkovich tip (E_{ind}) and the Poissons ratio were assumed to be 865 GPa and 0.2, respectively. The Poissons ratio of the sample (CNF) was assumed to be 0.3 (Roberts et al. 1994, Nakamura et al. 2004).

5.4 Morphology

Representative CNF samples were imaged using scanning electron microscope (SEM) and atomic force microscope (AFM). The SEM micrographs were obtained with a Hitachi TM3000 SEM at an acceleration voltage of 15.0 kV. Surface topography was measured with an MFP-3D AFM (Asylum Research). The specimens were dried as thin films on the stubs without using any adhesives and imaged 24 hours later. Images were obtained in an AFM chamber temperature of 25 °C using tapping mode (AC Mode) and an Asylum Research AC240TS-10 cantilever tip with a 9±2 nm radius with spring constant, k (N/m) =2 (0.5-4.4).

5.5 Statistical Analysis

The modulus (E), reduced modulus (E_R) and contact depth (h_c) data were compared by conducting a one-way Means/ANOVA to check if there was a significant overall difference (significance level (alpha) = 0.01). Significant different between groups were evaluated by use of a Tukey-Kramer Honestly Significant Differences (HSD) test with alpha=0.05. A sample size of six (n=60 for calibration and n=58 for CNFs tests) was used for all statistical analysis.

5.6 Results and Discussion

Results of the nanoindentation studies are presented in the following subsections.

5.6.1 Nanoindentations - Fused silica

A total of 60 indents were performed on different locations on the fused silica quartz sample for calibration (Figure 5.6).

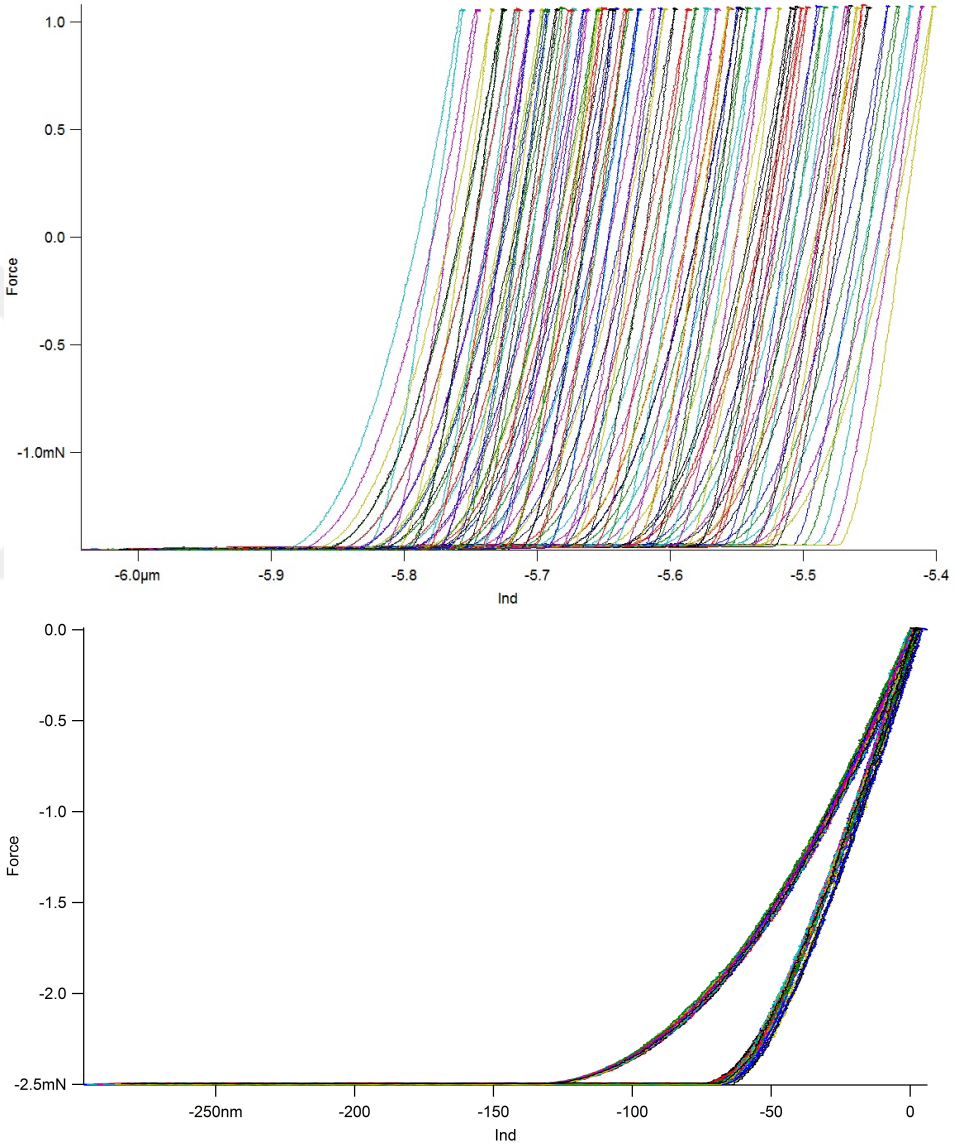

Figure 5.6: Total of 60 nanoindents' force – indentation curves.

a) Original curves. b) Curves after x-y offset.

The mean reduced modulus was calculated and statistically compared (Table 5.3). The results ranged from 83.54 GPa to 50.3 Gpa, with statistically significant differences from each method. It can be assumed and supported with Figure 5.2 that the imperfections on the tip surface and particles on the tip resulted in larger area calculations, with a corresponding lower predicted modulus.

Table 5.3: Calibration test results.

Calibration Method	N (number of indents)	H_c (Contact depth (nm)	Silica Modulus (GPa)
OP	60	67.8 (3.3)	83.54 (3.7) A
TI			50.30 (1.2) C
FS			71.91 (2.6) B

Parentheses indicate the coefficient of variation (COV, %). A, B, and C letters indicates the significant differences between the treatments.

According to obtained silica modulus results through OP approach, the polynomial correction function, which makes the silica modulus equal to a value between 68 GPa and 72 GPa, was created and the final silica modulus ended up with the 71.91 GPa modulus value for FS method. Also the silica modulus results through OP approach were calculated using actual area value obtained from the tip image for TI method (Table 5.3).

5.6.2 Nanoindentations - CNF

A total of 58 indents were performed on the CNF samples for the nanomechanical property investigations (Figure 5.7).

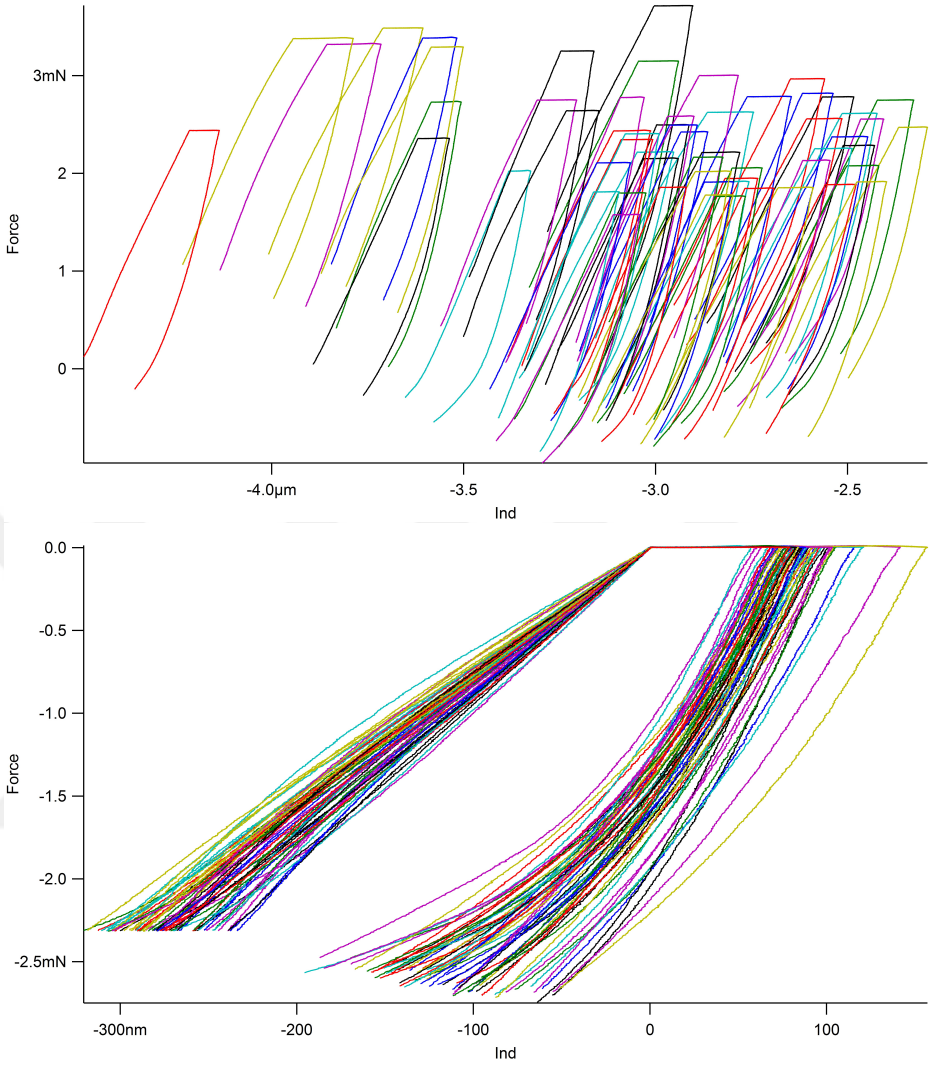

Figure 5.7: Collection of 58 nanoindents' force – indentation curves.

a) Original curves. b) Curves after x-y offset.

The CNF modulus, CNF reduced modulus, and the average contact depth values are summarized in Table 5.4.

The average modulus from the three methods ranged from 10.85 to 16.58GPa and reduced modulus ranged from 11.95 to 18.22 GPa. In both cases, the highest average value was from OP and the TI method provided the lowest value. The Coefficient of

Table 5.4: The nanomechanical properties of CNF.

Calibration Method	N (number of indents)	CNF Modulus (GPa)	CNF Reduced Modulus (GPa)	Hc, contact depth (nm)
OP	58	16.58 (16.9) A	18.22 (16.2) A	87.4 (16.3)
TI		10.85 (14.5) B	11.95 (14.2) B	
FS		15.79 (13.2) A	17.38 (12.9) A	

Parentheses indicate the coefficient of variation (COV, %). A and B letters indicates the significant differences between the treatments.

Variation results ranged from 12.9 to 16.9%, which were an order of magnitude higher than that for the fused silica. The increase in variability is expected attributable to the biological source of the CNF and minor variations in testing geometries associated with the developed technique. In contrast to results from the fused silica, there was no statistically significant difference between the OP and FS methods. Statistically, there was no significant difference between the OP and FS approach whereas the TI approach yielded a significantly lower value. This can be explained by the particles on the surface and tip imperfections. There are particles or dust on the tip surface that produce higher area calculations for the TI approach and resulted in lower modus values. However, these particles are not strong enough to create individual areas on the CNF samples during nanoindentation so the area created on the surface becomes very similar or the same as the Berkovich tip area. This explains why the OP and FS approaches produced similar results, as a result of having similar area calculations and values. The CNF reduced modulus estimates were consistently higher and followed the same estimate rankings by analysis techniques (i.e., 18.2 GPa for OP, 11.9 GPa for TI, and 17.4 GPa for FS) but following the same.

The author was not able to find any literature references that employed this technique on CNF for direct comparison; however, previous research has reported that the micro crystalline cellulose (MCC) and cellulose nano crystals (CNC) have modulus values ranges between 3 GPa and 25 GPa (Krishnamachari et al 2012, Wu et al. 2013, Wagner et al. 2011, Simonsen et al. 2012, Diddens et al. 2008, Lahiji et al. 2010 and Moon et al. 2014) and studies on cellulose microfibrils/nanofibrils indicated the CNF modulus values ranges between 6 GPa – 18 GPa (Saito et al. 2009, Iwamoto et al. 2007, Berglund et al. 2008, and Yano et al. 2004). The detailed CNF modulus value comparison (2004 to 2015) is provided in Table 5.5.

Table 5.5: Modulus value comparison with other studies.

Material	Test instrument	Test Method	E (GPa)	Researcher	Date
SWP	Instron	Bending	18	Yano et al.	2004
SWP	Instron	Tension	8.1	Iwamoto et al.	2007
MFC	Instron	Tension	10.4 - 13.7	Berglund et al.	2008
CNC	XRay	-	15	Diddens et al.	2008
HWP	Instron	Tension	6.2 – 6.5	Saito et al.	2009
CNC	AFM	Compression	18.1	Lahiji et al.	2010
CNC	AFM	Compression	8.1	Wagner et al.	2011
CNC	AFM	Compression	12.8	Simonsen et al.	2012
MCC	AFM - NI	Compression	3.5	Krishnamachari et al.	2012
CNC	Prediction	-	5.1	Wu et al.	2013
CNC	Theoretical	-	6.5-24.5	Moon et al.	2014
CNF	AFM - NI	Compression	15.8	Yildirim et al.	2015

SWP stands for softwood pulps and the HWP stands for hardwood pulps.

According to the detailed CNF modulus value comparison provided in Table 5.5, the CNF has similar or higher modulus values relative to CNC. Direct comparisons are difficult because of variations in test methods and equipment, also because of different raw materials or starting materials, moisture contents and different production processes; however, the strongest assumption is the region (Amorphous - Crystalline) that respond to external loads. In this research we assume that the nanoindents were created on CNF,

was responded by the crystalline region of the CNF's, where the CNFs crystallinity was earlier found varies between 73.3% and 82.1% (Peng 2013). According to Peng's research supercritical dried CNF has 73.3 % crystallinity, air dried CNF has 74.9 % crystallinity, freeze dried CNF has 80.7 % crystallinity and spray dried CNF has 82.1 % crystallinity, where freeze dried CNF showed high crystallinity. We wouldn't expect that high mechanical performance that we obtained in this study from the amorphous region of the CNF. It is same for other materials tested and reported in Table 5.5 and that is why similar or higher modulus values were obtained. Another study (Kumar et al. 2014) showed that the films produced using cellulose nanofibrils has Young's modulus varies between 5.5 GPa and 6.5 GPa, which was found comparable with our study. Kumar et al. applied a tension test to films, where the interaction between fibrils and the hydrogen bonding between each fibrils needs to be counted for final product performance which are the factors decrease the mechanical performance while switching from nano/micro to macro level.

A representative set of AFM and SEM images of the samples are given in Figure 5.8. As shown, there is variety in fibril diameters attributable to production process of CNF (mechanical grinding). The 3D AFM images are given in Figure 5.8a & 5.8b. The 2D SEM images are given in Figure 5.8c & 5.8d.

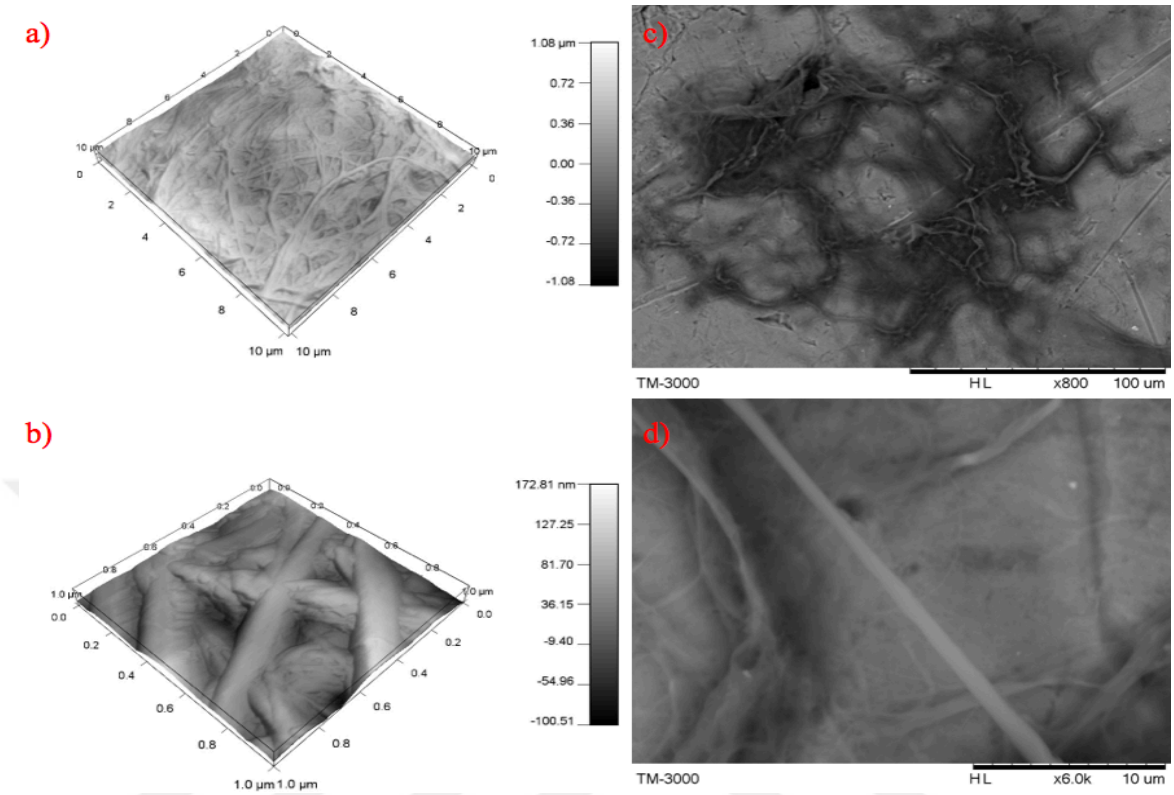

Figure 5.8: Representative AFM and SEM images of samples.

(a) AFM image of 100 µm2 scan area. (b) AFM image of 1 µm2 scan area. (c) SEM image of fibril distribution. d) SEM image of single microfibril and nanofibrils.

According to obtained 3D & 2D images (Figure 5.8) it can be assumed most of the nanoindents were applied to the fibrils with diameters in the range of several microns.

5.7 Conclusions

The cellulose nanofibrils investigated in this study had some variety based on their diameters. Because of this variety, more than 200 hundred nanoindentations were performed and only the successful indents, which had no slides, no cracks, no poor fit, and no strong adhesion through indentation process, were evaluated. The work performed in nanoscale needs extra attention to provide better accuracy, which is why three different

approaches were applied and the results were supported with the statistical analysis with low coefficient of variation values. The most accurate results were obtained from the FS approach because it is the only method that calculates the area according to area created on the sample (the actual area that responds to applied force). The FS method takes the imperfections into account and provides the actual area created on the surface. In this research, no significant differences were found between the OP approach and the FS approach; however, this doesn't mean or prove that the results will be same for any kind of material. These approaches were totally dependent on the material (material type, sample preparation, surface properties), tip (shape, imperfections), and also tip - material molecular attractions. It is strongly suggested to researchers to use the fused silica (FS) approach to reach more accurate results for measuring nanomechanical properties of any kind of material in their future investigations.

This research is a pioneering study where the most accurate CNF modulus results were discovered. Future work will include investigating the nanomechanical properties of the CNFs produced through different processes, from different raw materials, and under different conditions.

Acknowledgement

The authors thank University of Maine Process Development Center for supplying cellulose nanofibrils in this study. This work partly supported by the USDA/NIFA under the Wood Utilization Research Program (Project 2010-34158-21182)

CHAPTER 6

CONCLUSIONS AND RECOMMENDATIONS

6.1 Conclusions

CNF is a superb bio-based nanomaterial (bionanomaterial) that has great potential for use in the construction industry and the packaging industry as rigid foamed materials and panel boards. The ability to provide a CNF nanocomposite that provides excellent thermal insulation, and also eliminates the use of petroleum and has a lower carbon footprint, is ideally suited for the eco-conscious market of today. Following are conclusions of this study:

- CNF can be used for developing innovative products for building industry.
- CNF can be used as a matrix or reinforcing material in composite structures.
- Flexible or rigid products can be produced using cellulose nanofibrils.
- Corn starch can be used as a binder for cross linking purpose and is very compatible with CNF.
- The freeze-drying technique is suitable for product development starting with a CNF suspension.
- The nanomechanical properties (e.g., the role and effect of CNF in the composite structures) were characterized.
- Atomic Force Microscopy and Nanoindentation are the best methods to characterize the nanomechanical behavior of CNF.
- Different techniques were developed to understand the process and provide the most accurate results through nanoindentation.

- Also, the barrier properties of the cellulose nanofibrils were determined and needed suggestions are detailed under “Recommendations for future work” part.

6.2 Recommendations for Future Work

According to literature reviewed in this work, and additional research performed during this thesis proved that CNF has impressive physical, mechanical, nanomechanical, and thermal properties and is a very promising candidate to be a polymer of the future. Although these are remarkable properties, CNF has a huge potential for hydrophilicity and flammability, and is potentially suitable as a medium for growing mildew/mold. These are drawbacks for industry applications and further study will be needed to develop procedures and treatments to correct or reduce these properties.

6.2.1 Hydrophilicity and Silane Treatment

CNFs have free hydroxyl groups (OH-) in their chemical structure that make them a hydrophilic polymer, which means they easily interact with water. Without some protection, the material will break down quickly when moist and will lose its original material properties, including R-value, because the cells will collapse and the material structure will change. Silane treatment can solve this problem because fluoro-type or ethoxy-type silanes can create superb hydrophobic CNF-based composites.

The silane molecule includes super hydrophobic (water repellent) chemical groups in its structure. One side of the silane molecule (Si-O-CH3) will react with the free hydroxyl (OH) groups in cellulose nanofibrils, replacing the OH groups with the silane groups. The other side will repel the water molecules because each free hydroxyl group capable of making bonding with water molecules will be covered by silanes.

A representative diagram of the silane treatment process is shown in Figure 6.1. The condensation of ethoxy groups (O-CH3) results in polymerizing the silane around the cellulose. As a result of this mechanism, the byproduct will be an ethanol (HO-CH3) that is formed by attaching the ethoxy part of silane to the hydrogen atom of cellulose hydroxyl group.

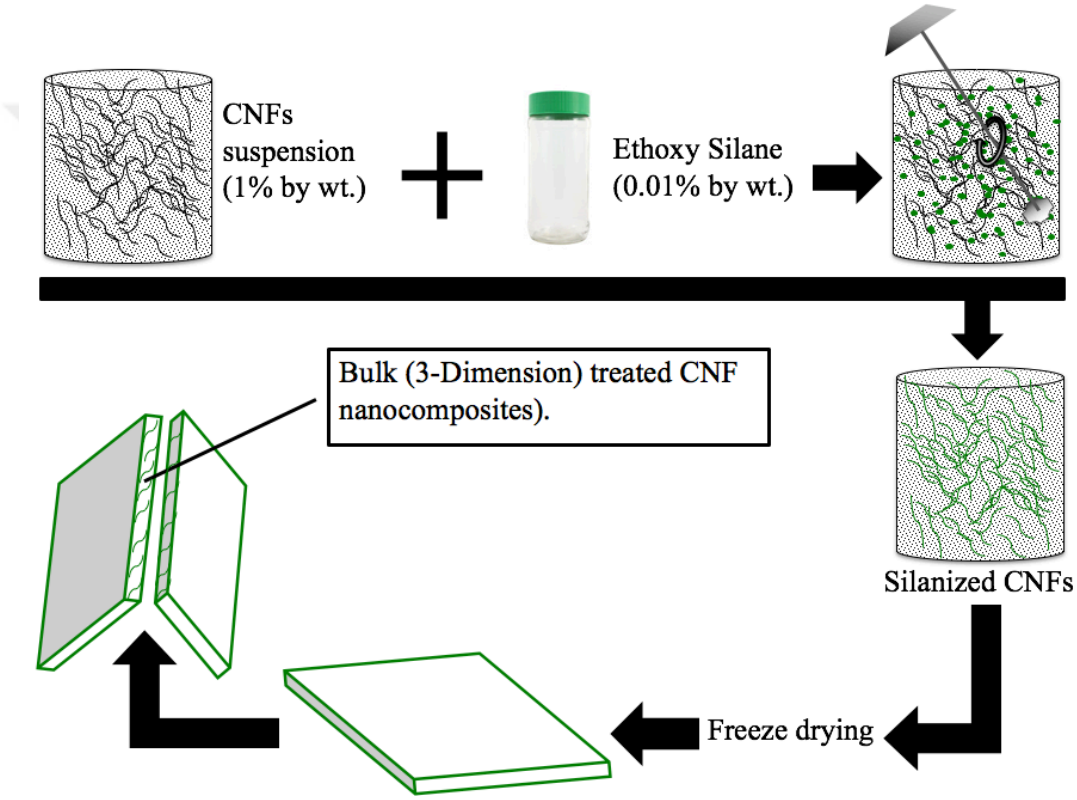

Figure 6.1: Silane treatment.

6.2.2 Flammability and Nanoclay Treatment

Cellulose is a polymer including thousands of $C_6H_{10}O_5$ molecules in its polymer chain. The atoms (C, H, and O) that create each molecule of the polymer chain will help start the combustion reaction. Combustion requires three components, fuel, oxygen, and energy (heat), and all three elements must be present for combustion to occur. When fuel reacts with oxygen, the heat energy produced breaks apart the original molecules, They

rejoin with the oxygen from the air and produce new molecules including water (H2O) and carbon dioxide (CO2). Clay or nanoclay can provide fire retardant property to CNF nanocomposites.

Nanoparticles are currently being added to nanocellulose-based materials to enhance barrier properties. The investigation of nanocomposites treated with clay/nanoclay received considerable and technological attention in recent years attributable to the impressive properties of clay. Nanoclays are good candidates for this project as they are compatible with CNF and can improve fire retardancy and possibly water resistance even if only used in small amounts (e.g., 1 to 5% total solid content by weight) (Fauze et al. 2013).

Traditional flame retardants work by depriving the system of at least one of the three needed components: fuel, oxygen, or heat. Certain flame-retardant materials have Thermal degradation temperatures (T_{deg}) of 400 °C or higher, depending on their specific makeup. These materials work by denying fuel to the combustion reaction because the material is not degrading. Most successful finishes on cellulose-based materials work by removing oxygen from the fire. Adding nanoclays to the CNF suspension will lower the T_{deg}, allowing for the rapid formation of a char layer. Char is not readily combustible and provides a barrier for the oxygen and heat to get to the material beneath it (Wakelyn et al. 1998 and Blanchard and Grave 2002).

Research shows that the introduction of clay to the CNF polymer allows for the formation of carbonaceous char in a nanocomposite, whereas the original polymer would not form a char layer (Gilman et al. 2001). Cellulose naturally forms a carbonaceous char during

combustion and, with the addition of the nanoclay particle, the creation and the amount of the char will be significantly increased. The formation of a substantial char layer will be an indicator of flame resistance.

The nanoclay treatment (Figure 6.2) will also likely reduce water absorption. The chemical structure of CNF has three hydroxyl groups (OH) available to bond with water molecules (H_2O). Nanoclay particles will bond to these available OH groups, decreasing their availability for bonding with water.

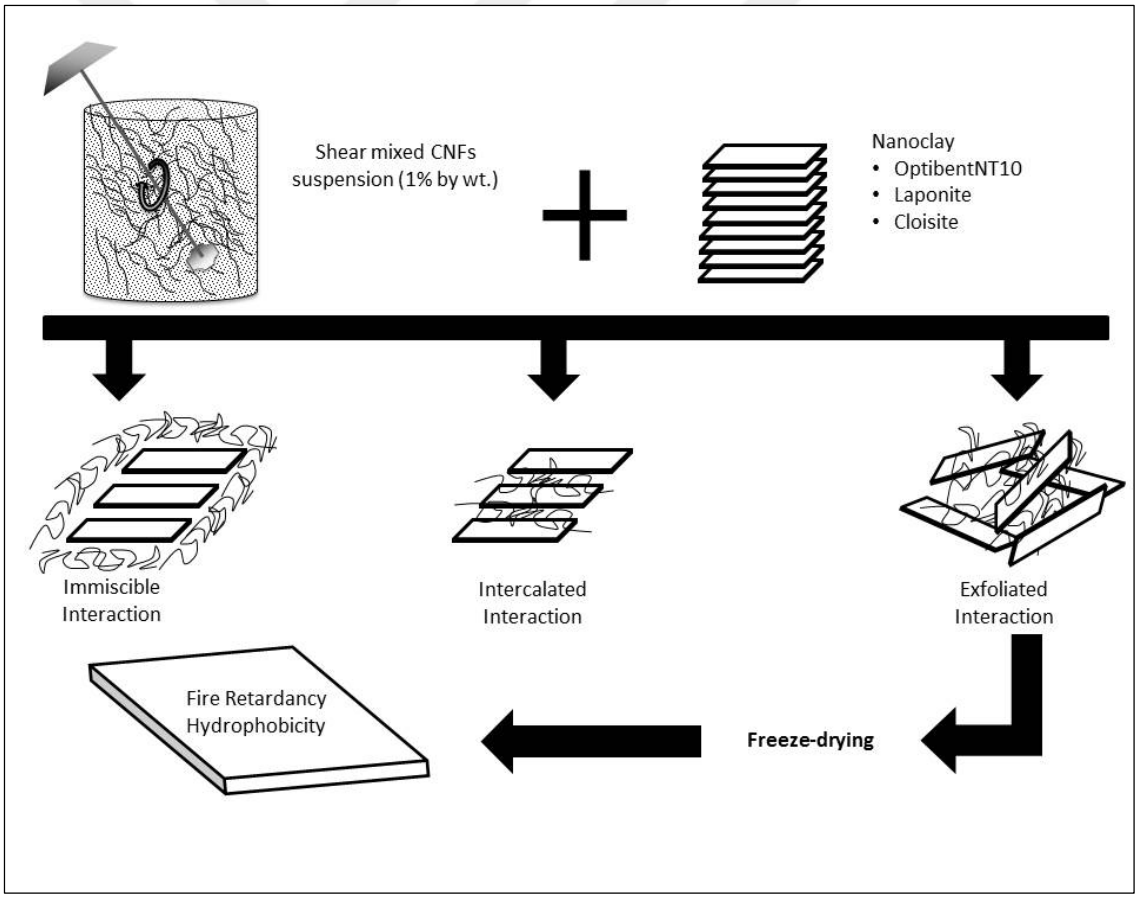

Figure 6.2: Nanoclay treatment.

Based on teleconferences with researchers from BYK Additives & Instruments and a deep literature review, Optibent NT10-, Cloisite-, and Lapotine-type nanoclays can be suggested to provide fire retardancy and potential hydrophobicity.

6.2.3 Mildew/Mold Growth and Prevention

Mildew and molds are forms of fungus and can be differentiated by their colors. Mildew appears white; mold can appear in shades of black, blue, red, or green. These simple microscopic organisms can thrive anywhere there is moisture. Molds are beneficial in nature where they help breakdown organic matter; however, they pose a significant problem indoors. Silane treatment or boric acid treatments can solve this problem; however, zinc oxide treatments may be another solution.

Growth of mildew and mold is directly related to moisture found in the medium. The nanoclay or silane treatment will potentially provide a strong barrier between the CNF nanocomposite structure and moisture, repelling water and preventing conditions for mold and mildew growth.

It is strongly believed that when the needed enhancements are done to eliminate or reduce the potential drawbacks of CNF that CNF-based nanocomoposites will be brought to the market safer and faster.

BIBLIOGRAPHY

A.N. Frone, S. Berlioz, J. F. Chailan, D. M. Panaitescu and D. Donescu (2011), Cellulose Fiber-Reinforced Polylactic Acid. Polymer Composites, 32: 976-985.

A. N. Nakagaito and H. Yano (2004), The effect of morphological changes from pulp fiber towards nano-scale fibrillated cellulose on the mechanical properties of high-strength plant fiber based composites. Applied Physics A. 78: 547-552.

Agarwal B.D. and Broutman L.J. 1980. Analysis and performance of fiber composites. New York, United States.

Ajayan P.M. and Tour J.M. (2007), Nanotube composites. Nature, 447(28): 1066-1068.

Ali Z.M. and Gibson L.J. (2013), The structure and mechanics of nanofibrillar cellulose foams. Soft Matter, 9: 1580-1588.

Arvidsson R., Nguyen D. and Svanstrom M. (2015), Life Cycle Assessment of Cellulose Nanofibrils Productions by Mechanical Treatment and Two different pretreatment processes. Environmental Science and Technology 49(11): 6881-6890.

Blanchard E.J. and Grave E.E. (2002), Polycarboxylic acids for flame resistant cotton/polyester carpeting. Textile Re. J. 72 (1): 39-43.

Briscoe B.J., Fiori L. and Pelillo E. (1988), Nano-indentation of Polymeric surfaces. J. Phys. D: Appl. Phys. (31): 2395-2405.

Butt H.J., Cappella B. and Kappl M. (2005), Force measurements with the atomic force microscope: Technique, interpretation and applications. Surface Science Reports 59(1-6): 1-152.

Cai Z., Rudie A.W., Stark N.M., Sabo R.C. and Ralph S.A. (2013), Chapter 6: New products and product categories" In the global forest sector: Changes, practices and prospects. Edited by Hansen E., Panwar R. and Vlosky R. 129-149. Boca Raton, FL: CRC Press.

Chen L., Gordon S. H., and Imam S.H. (2004), Starch Graft Poly(methyl acrylate) Loose-Fill Foam: Preparation, Properties and Degradation. Biomacromolecules, 5 (1): 238-244.

Cheng Q. and Wang S. (2008), A method for testing the elastic modulus of single cellulose fibrils via atomic force microscopy. Composites: Part A 39(12): 1838-1843.

Cheng Q., Wang S. and Harper D.P. (2009), Effects of process and source on elastic modulus of single cellulose fibrils evaluated by atomic force microscopy. Composites: Part A 40(5): 583-588.

Dri F. L., Hector J.L.G., Moon R.J. and Zavattieri P.D. (2013), Anisotropy of the elastic properties of crystalline cellulose Iβ from first principles density functional theory with Van der Waals Interactions. Cellulose 20(6): 2703-2718.

Dufresne A. and Vignon M.R. (1998), Improvement of Starch Film Performances Using Cellulose Microfibrils. Macromolecules, 31 (8): 2963-2696.

Eichhorn S.J. and Young R.J. (2001), The Young's modulus of a microcrystalline cellulose. Cellulose 8: 197-207.

Eichhorn S.J., Dufresne A., Aranguren M., Marcovich N.E., Capadona J.R., Rowan S.J., Weder C., Thielemans W., Roman M., Renneckar S., Gindl W., Veigel S., J. Keckes, Yano H., Abe K., Nogi M., Nakagaito A.N., Mangalam A., Simonsen J., Benight A.S., Bismarck A., Berglund L.A., Peijs T. (2010), Review: current international research into cellulose nanofibres and nanocomposites. Journal of Material Science 45 (1): 1-33.

Fauze A.A., Mattoso L.H.C. and Longo E. (2013) A simple procedure for the preparation of laponite and thermoplastic starch nanocomposites: Structural, mechanical and thermal characterizations. Journal of Thermoplastic Composite Material 26(1): 109-124.

Feynman R.P. (1992), There's Plenty of Room at the Bottom. Journal of Microelectromechanical Systems 1 (1): 60-66.

Gan Y.X., Chen C., Shen Y.P. (2005), Three-dimensional Modeling of the mechanical property of linearly elastic open cell foams. Internayional Journal of Solids and Structures 42(26): 6628-6642.

Gibson L.J., Ashby M.F., Schajer G.S. and Robertson C.I. (1982), The mechanics of two-dimensional cellular materials. Proc. R. Soc. Lond. A 382(1782): 25-42.

Gibson L.J. and Ashby M.F. (1998) Cellular Solids; Structure & Properties. Cambridge, United Kingdom.

Gilman, J.W., Kashiwagi T., Morgan A.B., Harris R.H., Brassell L., Awad W.H., Davis R.D., Chyall L., Sutto T., Trulove P.C., and DeLong H. (2001), Recent Advances in flame retardant polymer nanocomposites. Proceedings. Interscience Communications Limited. San Antonio, TX, pp 273-283 pp.

Gindl W., Konnerth J. and Schoberl T. (2006), Nanoindentation of regenerated cellulose fibers. Cellulose (13): 1-7.

Glenn G.M. and Wood D.I. (1995), Starch-Based Microcellular Foams. Carbohydrates, 72(2): 155-161.

Glenn G.M., Klamczynski A., Holtman K.M., Chiou B.S., Orts W.J., and Wood D. (2007), Cellulose Fiber Reinforced Starch-Based Foam Composites. Journal of Biobased Materials and Bioenergy, 1(3): 360-366.

Glenn G.M., Imam S.H., and Orts W.J. (2011), Starch-based foam composite materials: Processing and bioproducts. MRS Bulletin, 36: 696-702.

Gypsum Association (2010) Gypsum board typical mechanical and physical properties (GA-235-10) www.gypsum.org.

Hong C.Q., Han J.C., Zhang X.H. and Du J.C. (2013), Novel nanoporous silica aerogel impregnated highly porous ceramics with low thermal conductivity and enhanced mechanical properties. Scripta Materialia, 68(8): 599-602.

Hsu C.L. and Heldman D.R. (2004), Prediction models for the thermal conductivity of aqueous. International Journal of Food Science and Technology, 39(7): 737-743.

I. Diddens, B. Murphy, M. Krisch and M. Muller (2008), Anisotropic Elastic Properties of Cellulose Measured Using InelasticX-Ray Scattering. Macromolecules 41: 9755-9759.

Josefsson G., Berthold F. and Gamstedt E.K. (2014), Stiffness contribution of cellulose nanofibrils to composite materials. International Journal of Solids and Structures 51(5): 945-953.

Kalia S., Dufresne A., Cherian B.M., Kaith B.S., Averous L., Njuguna J. and Nassiopoulus E. (2011), Cellulose-Based Bio and Nanocomposites: A Review. International Journal of Polymer Science 2011: 1-35.

Krishnamachari P., Hashaikeh R., Chiesa M. and Gad El Rab K.R.M. (2012), Effects of Acid Hydrolysis Time on Cellulose Nanocrystals Properties: Nanoindentation and Thermogravimetrics Studies. Cellulose Chemistry and Technology 46 (1-2), 13-18.

Lahiji R.R., Xu X., Reifenberger R., Raman A., Rudie A. and Moon R.J. (2010), Atomic force microscopy characterization of cellulose nanocrystals. Langmuir 26 (6), 4480-4488.

M. Henriksson, L. A. Berglund, P. Isaksson, T. Lindstrom and T. Nishino (2008), Cellulose Nanopaper Structures of High Toughness. Biomacromolecules 9: 1579-1585.

Mahlia T.M.I., Taufiq B.N., Ismail, Masjuki H.H. (2007), Correlation between thermal conductivity and the thickness of selected insulation materials for building wall. Energy and Buildings, 39(2): 182-187.

Mallick P.K. (1993), Fiber-reinforced composites: materials, manufacturing and design-2nd ed. New York, United States.

Martins I.M.G., Magina S.P., Oliveira L., Freire C.S.R., Silvestre A.J.D., Neto C.P., Gandini A. (2009), New biocomposites based on thermoplastic starch and bacterial cellulose. Composite Science and Technology 69(13): 2163-2168.

Michalska M.J. and Pecherski R.B. (2003), Macroscopic Properties of Open-Cell Foams Based on Micromechanical Modeling. Technische Mechanik 23 (2-4): 234-244.

Moon R.J., Martini A., Nairn J., Simonsen J. and Youngblood J. (2010), Cellulose nanomaterials review: structure, properties and nanocomposites. Chem. Soc. Rev. 40 (7): 3941-3944.

Moran J.I., Alvarez V.A., Cyras V.P. and Vazquez A. (2008), Extraction of cellulose and preparation of nanocellulose from sisal fibers. Cellulose, 15(1): 149-159.

Nabar Y., Raquez J.M., Dubois P., and Narayan R. (2005), Production of Starch Foams by Twin-Screw Extrusion: Effect of Maleated Poly(butylene adipate-co-terephthalate) as a Compatibilizer. Biomacromolecules, 6(2): 807-817.

Nakamura K., Wada M., Kuga S. and Okano T. (2004), Poisson's Ratio of Cellulose Iβ and Cellulose II. Journal of Polymer Science Part B: Polymer Physics 42 (7): 1206-1211.

Naschie M.S.E. (2006), Nanotechnology for the developing world. Chaos, Solitons and Fractals, 30: 769-773

Nguyen D. (2014), Life cycle energy assessment of wood-based nanofibrillated cellulose. Master of Science Thesis. Chalmers University of Technology. Gothenburg, Sweden.

Oliver W.C. and Pharr G.M. (1992), An improved technique for determining hardness and elastic modulus using load and displacement sensing indentation experiments. J. Mater. Res. 7(6): 1564-1583.

Pakzad A., Simonsen J. and Yassar R.S. (2012), Gradient of nanomechanical properties in the interphase of cellulose nanocrystal composites. Composites Science and Technology, 72(2), 314-319.

Petersson L., Kvien I., Oksman K. (2007), Structure and thermal properties of poly(lactic acid)/cellulose whiskers nanocomposite materials. Composites Science and Technology, 67(11-12): 2535-2544.

Porter A.L. and Youtie J. (2009), How interdisciplinary is nanotechnology?. J. Nanopart Res., 11: 1023-1041.

Reuss, A. (1929), Calculation of the flow limits of mixed crystals on the basis of the plasticity of mono-crystals. Z. Angew, Math. Mech. 9: 49-58.

R. J. Roberts, R.C. Rowe and P. York (1994), The poisson's ratio of microcrystalline cellulose. International Journal of Pharmaceutics 105: 177-180.

Roco M. (2004), Nanoscale science and engineering: Unifying and transforming tools. AIChE Journal, 50 (5): 890-897.

S. Iwamoto, A. N. Nakagaito and H. Yano (2007), Nano-fibrillation of pulp fibers for the processing of transparent nanocomposites. Applied Physics A. 89: 461-466.

Sehaqui H., Zhou Q., Berglund L.A. (2011), High-porosity aerogels of high specific surface area prepared from nanofibrillated cellulose (NFC). Composites Science and Technology, 71(13): 1593-1599.

Shaler S.M., Lopez-Anido R. and Yildirim N. (2014), Cellulose Nanofibril (CNF) Reinforced Open Cell Foams; Application of Cubic Array Foam Theory, 57th SWST International Convention, Technical University in Zvolen, Zvolen, Slovakia, June 23-27 pp 451-458.

Shey J., Imam S.H., Glenn G.M., Orts W.J. (2006), Properties of baked starch foam with natural rubber latex. Industrial crops and products, 24(1): 34-40.

Shogren R.L., Lawton J.W., Doane W.M. and Tiefenbacher K.F. (1998), Structure and morphology of baked starch foams. Polymer, 39(25): 6649-6655.

Sinke H. Osong, Sven Norgren and Per Engstrand (2016), Processing of wood-based microfibrillated cellulose and nanofibrillated cellulose, and applications relating to papermaking: a review. Cellulose, 23: 93-123.

Siro I. and Plackett D. (2010), Microfibrillated cellulose and new nanocomposite materials: a review. Cellulose 17 (3): 459-494.

Svagan A.J., Samir M.A.S.A., and Berglund L.A. (2008), Biomimetic Foams of High Mecahanical Performance Based on Nanostructured Cell Walls Reinforced by Native Cellulose Nanofibrils. Advanced Materials, 20(7): 1263-1269.

Svagan A.J., Berglund L.A., and Jensen P. (2011), Cellulose Nanocomposite Biopolymer Foam-Hierarchical Structure Effects on Energy Adsorption. Applied Materials & Interfaces, 3(5): 1411-1417.

T. Saito, M. Hirota, N. Tamura, S. Kimura, H. Fukuzumi, L. Heux and A. Isogai (2009), Individualization of Nano-sized Plant Cellulose Fibrils by Direct Surface Carboxyaltion Using TEMPO Catalyst under Neutral Conditions. Biomacromolecules 10: 1992-1996.

Tatarka P. D. and Cunningham R. L. (1996), Properties of Protective Loose-Fill Foams. Journal of Applied Polymer Science, 67 (7): 1157-1176.

V. Kumar, R. Bollstrom, A. Yang, Q. Chen, G. Chen, P. Salminen, D. Bousfield and M. Toivakka (2014), Comparison of nano- and microfibrillated cellulose films. Cellulose 21, (5): 3443-3456.

Wagner R., Moon R.J., Pratt J., Shaw G. and Raman A. (2011), Uncertainty quantification in nanomechanical measurements using the atomic force microscope. Nanotechnology 22, (45): 5703-5711.

Wakelyn P.J., Bertoniere N.R., French A.D., Thibodeaux D.P., Triplett B.A., Roussele M.A., Goynes W.R., Edwards J.V., Hunter L., McAlister D.D. and Gamble G.R. (1998), “Chapter 9: Cotton Fibers.” In Handbook of Fiber Chemistry, Second Edition, edited by M. Lewin and E.M. Pearce. Boca Raton, FL: CRC Press.

Wang X., Zhong J., Wang Y. and Yu M. (2006), A study of the properties of carbon foam reinforced by clay. Carbon, 44(8): 1560-1564.

Wu X., Moon R.J. and Martini A. (2013), Crystalline cellulose elastic modulus predicted by atomistic models of uniform deformation and nanoscale indentation. Cellulose (20): 43-55.

Wu X., Moon R.J. and Martini A. (2014), Tensile strength of Iβ crystalline cellulose predicted by molecular dynamics simulation. Cellulose (21): 2233-2245.

Yang H., Yan R., Chen H., Lee D.H. and Zheng C. (2007), Characteristics of hemicellulose, cellulose and lignin pyrolysis. Fuel, 86(12-13): 1781-1788.

Yildirim N., Shaler S.M., Gardner D.J., Rice R. and Bousfield D.W. (2014), Cellulose Nanofibril (CNF) Reinforced Starch Insulating Foams. Cellulose 21(6): 4337-4347.

Yildirim N., Shaler S.M., Gardner D.J., Rice R. and Bousfield D.W. (2014), Cellulose Nanofibril (CNF) Reinforced Starch Insulating Foams. MRS Proceedings, (1621); 177-189.

Yildirim N., Shaler S.M., Gardner D.J., Bousfield D.W. and Rice R. (2013), Cellulose Nanofibril (CNF) Insulating Foams, Contributing Author, Production and Applications of Cellulose Nanomaterial, Author: Michael T. Postek, Robert J. Moon, Alan W. Rudie, Michael A. Bilodeau, ISBN: 978-1-59510-224-9.

Yildirim N. and Shaler S.M. (2015), Nanomechanical properties of cellulose nanofibrils (CNF), “MRS Advances”, DOI: http://dx.doi.org/10.1557/adv.2015.30, 2015.

Yucheng Peng (2013), Cellulose nanofibrils drying and their utilization in reinforcing thermoplastic composites, Ph.D. Thesis, The University of Maine, Orono, ME.

BIOGRAPHY OF THE AUTHOR

Nadir Yildirim was born in Turkey in 1985. He attended to Karadeniz Technical University in Trabzon, Turkey and received his B.Sc. in Forestry Industrial Engineering in 2007. In the same year, his exam scores ranked first in the Wood Science and Furniture area and he was awarded a full scholarship for post-graduate studies at Mugla University, Mugla, Turkey. Mr. Yildirim received his M.Sc. in 2010 in Forestry Industrial Engineering and ranked first in Faculty of Technology.

Later that year Mr. Yildirim temporarily moved to the United States to conduct research in wood composite panels at Purdue University. Moving back to his home country, he taught at Mugla University for one year.

In 2011, Mr. Yildirim again moved to the United States to begin a position as a graduate research assistant at the University of Maine's Advanced Structures and Composites Center while pursuing doctoral studies. In 2014, he graduated from the University of Maine's Innovation Engineering Program.

Nadir Yildirim, established his own research and product development company in 2014, Revolution Research Inc. (RRI), and has been working with advanced nanocomposites. He has been Program Manager for several development projects in composites and advanced materials, including studies of water repellent nanocellulose composites, starch foams, nanocellulose foam boards, and eco-friendly thermal insulation composite foam boards. In 2016 RRI received a National Science Foundation STTR grant award and also several Maine Technology Institute (MTI) grants to develop nanocellulose composite commercial products. RRI has also submitted an application to the U.S. Environmental

Protection Agency for a grant focusing on development of building materials using nanocellulose; award is expected in August 2016.

Mr. Yildirim is a candidate for the Doctor of Philosophy degree in Forest Resources from the University of Maine in August 2016.